Title
DESIGN THEORY AND SEPARATIONS IN PREPARATIVE-SCALE CONTINUOUS-FLOW ANNULAR-BED ELECTROPHORESIS

Authors
Vermeulen, Theodore
Nady, Louie
Kroehta, John M.
et al.

Publication Date
1970-10-01

Submitted to Industrial and Engineering
Chemistry Process Design and Development
Quarterly

UCRL-19981
Preprint

c. 2

DESIGN THEORY AND SEPARATIONS IN PREPARATIVE-SCALE CONTINUOUS-FLOW ANNULAR-BED ELECTROPHORESIS

Theodore Vermeulen, Louie Nady, John M. Krochta,
Edo Ravoo and Darryl Howery

October 1970

AEC Contract No. W-7405-eng-48

LAWRENCE RADIATION LABORATORY
UNIVERSITY of CALIFORNIA BERKELEY

DISCLAIMER

DESIGN THEORY AND SEPARATIONS IN PREPARATIVE-SCALE CONTINUOUS-FLOW ANNULAR-BED ELECTROPHORESIS

Theodore Vermeulen, Louie Nady, John M. Krochta, Edo Ravoo[1] and Darryl Howery[2]

Department of Chemical Engineering and Lawrence Radiation Laboratory, University of California, Berkeley, Calif. 94720

ABSTRACT

A cylindrical electrophoresis column with electrodes at the center and at the outer circumference, with lengthwise flow through either inert or adsorbent packing, can be used for continuous fractionation of ionic solutes on a scale approaching kilograms per hour. A feed mixture is fed in a ring of specified radius at the upstream end, and solute fractions are withdrawn from eight concentric rings at the downstream end. The constant-property design theory for such an apparatus is reviewed and extended with particular emphasis on heat dissipation and radial dispersion. Master plots are given to estimate temperature profiles for given column geometry and operating conditions. Constructional features of the separation unit and of the many auxiliary components are described. Trial separations of dye mixtures and of amino acid mixtures illustrate the feasibility of the present pilot-scale unit.

---

[1]Present address, Afdeling Chemische Technologie, Technische Hogeschool Twente, Enschede, The Netherlands.

[2]Present address, Department of Chemistry, Brooklyn College of the City University of New York, Brooklyn, N. Y.

enters in a narrow band at r_F at the top of the column. Application of an appropriate voltage (say 25-100V, based on concentration level and flow rate in the bed) causes ionic solutes to change their radial positions as they travel down the column. Solutes with differing electrochemical mobilities follow different paths and emerge at the outlet at the bottom of the column in separate rings of radius r_L. A background electrolyte ("elutant") is fed downward continuously and uniformly across the entire bed cross-section. The ionic components of the feed follow paths resulting from an axial vectorial component determined by

convective transport due to bulk elutant flow and chromatographic retardation if the packing is sorbent, and from

a radial component determined by the electrolytic migration in solution, chromatographic retardation for non-inert packing, and electrolytic migration of ions on packing with ion-exchange sites. In steady-state operation the solute is collected continuously at the downstream end in a segmented offtake arrangement.

To remove oxygen and hydrogen gas generated during elctrolysis and to extract a part of the heat produced within the packed bed and diaphragms, a conducting aqueous solution ("coolant") is circulated rapidly through each of the electrode compartments.

Cylindrical geometry was selected for scale-up because of the relative ease of construction and the absence of bed face effects. The thermal field, like the electric-potential field, is cylindrically symmetric under ideal performance. Porath (1957) has analyzed the temperature distribution in a zone-electrophoresis apparatus with peripheral cooling similar to that described here. The maximum permissible temperature is dictated by either the thermal stability of the materials undergoing separation or the need to avoid vapor formation in the bed.

Too great a radial spread of bands can prevent separation; the range of satisfactory operating conditions may be widened by using a smaller packing diameter.

The physical variables which influence the extent of separation thus include the geometry of the unit, the thermal and electrical properties of all components between the electrodes, and the chromatographic properties, geometry, and size of the packing. For a given unit and maximum allowable temperature, one must choose the best combination of voltage, elutant composition, and residence times. Certain design considerations for the annular-bed unit have been given by Hybarger *et al.* (1963) and Ravoo *et al.* (1967). In the present paper, the design theory is reviewed and extended, and the important constructional features and operational procedures of the Berkeley annular-bed unit are detailed.

DESIGN-CALCULATION METHODS

Current and Heat Flux in Cylindrical Geometry

Because the apparatus is presumed to have circular symmetry in the thermal and electric fields at all heights in the bed, physical properties can be considered uniform over any circle centered about the axis of the column. The local current density i is given by the Ohm-Fourier law of electrical conduction:

$$i = -k_m \left[\left(\frac{\partial E}{\partial r}\right)^2 + \left(\frac{\partial E}{\partial y}\right)^2\right]^{1/2} \tag{1}$$

where E is the potential, r the radius, y the axial depth, and k_m the local effective electrical conductivity (which is a function of the local temperature on a circle with coordinates r,y). The power density is therefore

$$\vec{i}\cdot\vec{\nabla}E = -k_m\left[\left(\frac{\partial E}{\partial r}\right)^2 + \left(\frac{\partial E}{\partial y}\right)^2\right] \tag{2}$$

For a cylindrical volume element $2\pi r\ dr\ dy$, the most general form of the heat balance is

$$\frac{1}{r}\frac{\partial}{\partial r}\left(rk_h\frac{\partial T}{\partial r}\right) + \frac{\partial}{\partial y}\left(k_h\frac{\partial T}{\partial y}\right)$$

$$-\frac{\partial}{\partial r}\left(rU_r\rho c_p T\right) - \frac{\partial}{\partial y}\left(U\rho c_p T\right) + \vec{i}\cdot\vec{\nabla}E = \frac{\partial}{\partial t}\left(\rho c_p T\right) \tag{3}$$

where k_h is the effective thermal conductivity, ρ the density of the process stream, c_p the heat capacity of the process stream, t the time, U_r the linear velocity of the fluid in the radial direction, and U the linear velocity of the elutant in the axial direction.

The first and second terms in Equation 3 represent heat conduction in the radial and axial direction respectively; the third and fourth terms heat convection radially and axially respectively; and the right-hand term heat accumulation with time. The heat generation term is given by Equation 2.

Practical Relations. For practical continuous electrophoresis, Equation 3 can be simplified considerably. In the steady state, heat accumulation disappears. Axial conduction of heat will usually be small compared with convection. Radial convection, as from electro-osmosis, can usually be neglected. Density and heat capacity can usually be considered constant. The axial voltage-gradient $(\partial E/\partial y)$ is neglected. Finally, a plug-flow model is adopted, characterized by a uniform flow in the axial direction ($U = y/\tau$, with residence time τ proportional to y) and consequent zero flow in the radial direction.

With all these assumptions, Equation 3 simplifies to

$$\frac{1}{r}\frac{\partial}{\partial r}\left(rk_h\frac{\partial T}{\partial r}\right) - \rho c_p\frac{\partial T}{\partial \tau} - k_m\left(\frac{\partial E}{\partial r}\right)^2 = 0 \qquad (4)$$

Both k_h and k_m are temperature-sensitive. Their temperature dependence can be either approximated by average values over the experimental temperature range (the "constant-property case"), or calculated from point-by-point temperature profiles. Both constant-property and variable-property cases will be considered here. Frequently, the total concentration varies widely, and affects k_m; here it is assumed that the elutant species level is large, and gives nearly uniform k_m throughout.

The simplest boundary conditions for Equation 4 are the following: the temperatures of the inner and outer cylindrical walls of the separation chamber (including the diaphragms) remain constant and equal to the temperature T_o of the entering process stream; a constant voltage-difference E_{ab} is applied radially along the entire length of the separation chamber. Algebraically

$$\tau = 0: \qquad T = T_o$$
$$r = r_b: \qquad T = T_o,\ E = 0$$
$$r = r_a: \qquad T = T_o,\ E = E_{ab}$$

Coordinates r_b and r_a denote the inner and outer radii of the packed bed. Additional voltage-difference across the diaphragms is neglected.

Expanding the first term in Equation 4, setting $\kappa = k_m/k_h$, and introducing relative coordinates for radius ($r' = r/r_b$), electrical potential ($E' = E/E_{ab}$), and temperature variable $T' = T - T_o$, convert Equation 4 to the form:

$$\frac{\partial^2 T'}{\partial r'^2} + \frac{1}{r'}\frac{\partial T'}{\partial r'} + \frac{1}{k_h}\frac{\partial T'}{\partial r'} \cdot \frac{\partial k_h}{\partial r'} - \frac{c_p \rho r_b^2}{k_h}\frac{\partial T'}{\partial \tau} - \kappa E_{ab}^2 \left(\frac{\partial E'}{\partial r'}\right)^2 = 0 \qquad (5)$$

with the boundary conditions

$$\tau = 0: \qquad T' = 0$$
$$r' = 1: \qquad T' = 0,\ E' = 0$$
$$r' = r_a/r_b = r_o' \qquad T' = 0,\ E' = 1$$

Two solutions of this problem, which involve different treatments of k_h and k_m, will now be discussed.

<u>Solution for Constant Physical Properties</u>. The treatment of Hybarger <u>et al</u>. (1963) will now be reviewed and extended. With uniform electrical conductivity, the local voltage in the bed is a function of radial position only. In circular geometry, with constant total radial flow of current, the local current controls the voltage gradient. For uniform conductivity, then, the voltage gradient will vary with the radius:

$$\frac{dE}{dr} = (\text{const})\ \frac{1}{r} = \frac{E_{ab}}{\ln(r_a/r_b)} \cdot \frac{1}{r} \tag{6}$$

Here the constant has been evaluated by integrating the gradient over the entire annulus to which the known voltage difference E_{ab} is applied. Hence, in dimensionless variables,

$$\frac{dE'}{dr'} = \frac{1}{r'\ln r'_o} \tag{6a}$$

Also, k_h is assumed constant, hence Equation 5 reduced to

$$\frac{\partial^2 T'}{\partial r'^2} + \frac{1}{r'}\frac{\partial T'}{\partial r'} - \frac{r_b^2}{\alpha_h}\frac{\partial T'}{\partial \tau} - \frac{\kappa E_{ab}^2}{r'^2(\ln r'_o)^2} = 0 \tag{7}$$

where α_h (= $k_h/\rho c_p$) is the thermal diffusivity.
The analytical solution for Equation 5 has been given in terms of a dimensionless temperature rise:

$$\Theta = \frac{T'}{\kappa E_{ab}^2} = \frac{1}{2}\left\{\frac{\ln r'}{\ln r'_o} - \left(\frac{\ln r'}{\ln r'_o}\right)^2\right\}$$

$$- \sum_{j=1}^{\infty} A'_j\ \Phi \exp\left(-\lambda_j^2\ \alpha_h\ \tau/r_b^2\right) \tag{8}$$

with

$$\Phi = Y_o(\lambda_j)\cdot J_o(\lambda_j r') - J_o(\lambda_j)\cdot Y_o(\lambda_j r') \tag{9}$$

J_o and Y_o denote zero-order Bessel functions of the first and second kinds. The eigenvalues λ_j are roots of

$$Y_o(\lambda_j)\cdot J_o(\lambda_j r_o') - J_o(\lambda_j)\cdot Y(\lambda_j r_o') = 0 \tag{10}$$

and the coefficients A_j' can be calculated from

$$A_j' = \frac{\int_1^{r_o'} \Phi\left\{\frac{\ln r'}{\ln r_o'} - \left(\frac{\ln r'}{\ln r_o'}\right)^2\right\} r'dr'}{2\int_1^{r_o'} \Phi^2 r'dr'} \tag{11}$$

Equation 8 was evaluated manually for $r_o' = 8$, to match the geometry of the experimental unit (but including the diaphragms). For more general use in the design of a cylindrical electrophoretic apparatus, a complete family of temperature profiles (Θ vs r) has been computed numerically, for varying values of $\alpha_h\tau/r_b^2$, using an IBM 7090 digital computer over a range of radius ratios from $r_o' = 1$ (flat-slab geometry) to $r_o' = \infty$ (axial line-source). In this calculation the λ_j were determined with 6-figure accuracy by an iteration technique; the A_j' were evaluated to 5-decimal accuracy by numerical integration. Four-figure accuracy for Θ was obtained by truncating the series in Equation 8 after $j = 10$; in most cases, three-figure accuracy in Θ could be achieved by truncating at $j = 4$. The dimensionless temperature coordinate Θ ($= k_h T'/k_m E_{ab}^2$) replaces the previously-used dimensionless coordinate

$k_h T'Q$; now $\Theta = [k_h T'/Q]/(\ln r_o')^2$, because $Q \equiv k_m E_{ab}{}^2/(\ln r_o')^2$. Figure 2 shows Θ vs r' for $r_o' = 8$.

In order to generalize the curves for individual radius-ratios and to provide a rapid and reasonably accurate estimation of temperatures, the computed results are summarized in two master plots. Figure 3a correlates the peak temperature expressed as Θ_p and the radial position r_p' of the peak, as functions of the r_o' and $\alpha_h \tau/r_b{}^2$ contours which characterize the column. Figure 3b enables one to estimate T'/T_p' for each desired value of r, and hence calculate T. The graphical correlation is accurate to within 10% of T'/T_p', and thus lies within the usual range of the assumptions and the input data.

An example of the use of Figures 3ab will now be given, based on typical data from the Berkeley cylindrical column: r_a = 10 cm, r_b = 1.25 cm, $k_h = 2.1 \times 10^{-3}$ cal/cm sec°C $= 8.8 \times 10^{-3}$ watt/cm^3, c_p = 1.0 cal/g°C, τ = 7200 sec, T_o = 25°C, and E_{ab} = 40 volts. In Fig. 3a the $r_a/r_b = 8$ curve intersects the curve for $\alpha_h \tau/r_o{}^2 = 10$ (which approximates the actual value of 9.7) at the coordinates $(r_p - r_b)/(r_a - r_b) = 0.24$, $\Theta_p = 0.11$. Thus $r_p = 3.35$ and T_p = 41.0°C. From these, the temperature at any radius, say r = 5 cm, can be found. The right-hand plot in Figure 3b, with the contour value $(r_p - r_b)/(r_a - r_b) = 0.24$ and the abscissa value $(r - r_p)/(r_p - r_b) = 0.79$ gives by interpolation $(T - T_o)/(T_p - T_o) = 0.26$, or T = 29.2°C.

The schematic relation of the theoretical framework to actual operating conditions can be explored further by reference to Figure 4. In a given apparatus, for constant thermal conductivity of bed, constant specific conductance of solution, and a fixed maximum temperature, the allowable power density is high at the shortest residence times and declines asymptotically to a constant-Q contour for long residence times. Power density is proportional to concentration times the square of the applied voltage. The problem is to determine what combination of concentration, voltage, and residence time will provide the maximum production rate (proportional to voltage times concentration). For long-term continuous operation, this rate occurs at the largest allowable power density and the largest allowable concentration. It corresponds to a long residence time, and hence to a low voltage. (The straight-line contours for constant power density Q and constant production rate P, shown in separate areas of the diagram for clarity, actually extend across the entire diagram.)

For short-term or intermittent operation, the allowable residence time will have practical limitations, since at least one residence time is lost in each start-up.

If the solutes involved are heat-sensitive, the residence time will become a factor in determining the allowable temperature rise, and then the allowable power-density curve will decrease steadily for increasing residence times, rather than becoming constant. (Thus the dashed curve will then be replaced by a curve which is steeper at all concentrations.)

The energy consumption per unit quantity of feed (or product), $Q\tau/P$, is constant (= 4) at all points in Figure 4. Thus only the amortized apparatus cost per unit of product will vary as the production rate varies.

<u>Electromigration and Dispersion of Solute</u>

Electromigration in the direction perpendicular to flow has the objective of resolving a mixture of solutes into a number of bands centered at different radii, each containing an individual component. The greater the difference in mobilities of two solutes is, the less the displacement of the slower-moving one that will give the needed separation distance between the centers of the solute bands. This separation distance is determined by several factors: the width of the offtake rings, and their positions relative to the feed ring; the initial width of the mixed-solute feed band; and the dispersive spreading which occurs radially as the solutes flow axially through the packed bed.

The rate of radial movement of a solute A is given by the product of its mobility u_A and the voltage gradient:

$$\frac{dr_A}{dt} = u_A \frac{dE}{dr} \tag{12}$$

Substitution from Eq. (6), with integration between the feed radius r_F and the radius r_A to which A has been displaced, yields

$$\frac{r_A^2 - r_F^2}{2} = u_A \tau \frac{E_{ab}}{\ln(r_a/r_b)} \tag{13}$$

If this is combined with the corresponding relation for another solute B, the result is

$$\frac{r_A^2 - r_B^2}{2} = (u_A - u_B)\tau \frac{E_{ab}}{\ln(r_a/r_b)} \tag{14}$$

Thus, as Ravoo <u>et al</u>. (1967) have indicated, the product of E_{ab} and τ determines the separation distance; for a given distance, E_{ab} can be reduced if τ is increased, or vice versa.

Radial dispersion, which produces transverse spreading of the bands, will often be the limiting factor in determining the efficiency of a separation. Since the effect is short-range, the analysis is simplified by assuming rectangular geometry. In the analysis of this spreading, the feed mixture of solutes is considered to enter the packed bed from a semi-infinite slot of infinitesimal width. For rectangular or near-rectangular geometry, the spreading process is described by the relation

$$D_r \frac{\partial^2 C}{\partial r^2} - U \frac{\partial C}{\partial y} = 0 \qquad (15)$$

At flowrates greater than 10^{-2} cm/sec, molecular diffusivity is much less than the eddy diffusion arising from hydrodynamic flow, and hence the radial-dispersion rate is directly proportional to U. The Gaussian-form solution, based upon a point source, is given in terms of a horizontal band width s at the bottom of the column that contains concentration levels above any particular specified value C:

$$s^2 = 1.32\ d_p L\ ln \frac{C_m}{C} \qquad (16)$$

The maximum concentration C_m is given by the relation

$$C_m = (q/U) \left[3/(\pi d_p)\right]^{1/2} \qquad (17)$$

where d_p is the average diameter of the packing, q is the total quantity of the solute fed per unit length of feed line per unit time, and the constant is based on a radial Péclet number (d_pU/D_r) equal to 12. The fraction C/C_m determines the recovery of a product over a specified offtake distance (see Figure 5). For example, C/C_m values of 0.05 and 0.10 correspond approximately to 99% and to 98% recovery of a component. Eq. (16) has been amply verified on a smaller rectangular unit (Nady, 1965).

For values of $C/C_m = 0.05$, s = 1.0 cm (a sufficiently narrow band), and a column length of 120 cm (as for the Berkeley unit), then $d_p = 0.002$ cm. This means that, to prevent overlap of bands, a packing of quite small diameter must be used. The band as fed has a finite width which makes the entrance level behave as if it were a distance ΔL downstream from a point source. For example, if the feed width = 0.40 cm, $C/C_m = 0.10$, and $d_p = 0.010$ cm (a readily available packing size), then ΔL, the correction to L, is 5.2 cm. The effective L is then (120 + 5.2) cm. For L = 125.2 cm, $C/C_m = 0.10$ and $d_p = 0.010$, the calculated band width is 2.59 cm. Since the width of each of the eight collecting rings at the outlet of the column to be described in the next section is 0.95 cm, the spreading should not prevent a high-purity binary separation.

A more exact treatment of radial dispersion involves explicit inclusion of feed band width and cylindrical geometry (Vermeulen and Tobias, 1965). However, the approximate treatment just outlined is simpler to use and gives adequate accuracy in most applications.

Solution for Temperature-Dependent Physical Properties

Even in cases where the temperature dependence of k_h and k_m is known, an analytical solution to Eq. (5) usually is unattainable. Since the behavior of $k_h(T)$ and $k_m(T)$ is highly dependent upon the exact nature of the system, any numerical solution will inherently be specific to a particular operation, and the relation between power input and the desired separation distance must be determined by carrying out an iterative solution. A complete computer program for beds having nonuniform physical properties is available (Masson and Kavanaugh, 1965).

For this analysis Equations 12 and 16 are replaced by the following generating differential equation which is solved simultaneously with Equation 5 by a finite-difference procedure:

$$\frac{\partial}{\partial r}\left(rD_r \frac{\partial C}{\partial r}\right) + \frac{\partial}{\partial r}\left(ruC \frac{\partial E}{\partial r}\right) - U \frac{\partial}{\partial y}(rC) = 0 \qquad (18)$$

where D_r is the radial diffusivity and C is the normal concentration of the particular component. The terms in Equation 18 account respectively for radial diffusion, electromigration, and axial convection. The assumptions involved in Equation 18 are that axial diffusion is small compared to axial convection, axial electrophoretic migration is negligible, the column operates at steady state, each component migrates independently, and electroosmosis is negligible.

A computer simulation involving separation of the amino acids leucine and phenylalanine has been used to test and illustrate this approach (Vermeulen and Tobias, 1965).

APPARATUS

A flow diagram for the continuous electrophoresis unit showing the accessory equipment is given in Figure 6. The relatively intricate and well-coordinated apparatus which is described briefly here has evolved through several phases (Vermeulen and Tobias, 1962-66; Howery and Vermeulen, 1964). The separation unit proper, shown in Figure 7, is 9 inches in diameter and 48 inches high. To permit continuous use for extended periods, storage drums for feed (2 gallons /), elutant (15 gallons /), and coolant (50 gallons /) are provided. A degasifier and heat exchanger for the coolant, a sampling rack, D.C. voltage supply, and a control panel for flowrate control comprise the major auxiliary components.

Separation Unit

The separation column, along with the auxiliary equipment, is mounted within a stand built from Dexion structural-steel slotted angle bars. An outer cover of commercial flanged glass pipe (Q.V.F., Ltd., London) provides electrical insulation, as well as visibility into the outer electrode compartment.

The electric current flows between two concentric electrodes: an axially centered gold-plated nickel rod 0.50 inches in diamter, and an outer perforated sheet (0.50-inch holes covering 45% of total area) of 28-gauge Hastelloy B (67% nickel, 28% molybdenum, and 5% iron), rolled to

8.25-inch diameter. Diaphragms of porous siliceous ceramic (Filtros 35, Electro Refractories, East Rochester, N. Y.) confine the packed bed while allowing electrical conduction. The inner diaphragm has a 1-inch inside diameter and a wall thickness averaging 0.188 inch. The outer diaphragm is of the same wall thickness and is 8 inches in outside diameter. Each diaphragm is composed of two 2-foot sections (the largest available) joined with epoxy-resin glue (Electrochemical Adhesive M-648-W). The diaphragms also have glued on Teflon and Neoprene gaskets which serve as seals at the top and bottom of the column. Because the siliceous diaphragms caused pronounced electro-osmotic flow, the outer diaphragm has been pretreated with a lubricating-oil additive (Oloa 1200, Chevron Research Corp.) applied as a 2% solution in hexane. In preliminary tests, electroosmosis was reduced by up to 85%; the coating appears stable when soaked in buffered solutions.

Two packings have been used: 170- to 230-mesh glass beads ("Superbrite" no. 150, 0.003 inch mean diameter, 3M Manufacturing Co.), and 100- to 150-mesh crosslinked polystyrene beads (0.005 inch mean diameter, Dow Chemical Co.). The packing material is supported above the offtake plate by a polypropylene filter screen (Polymax-B No. 3449, National Filter Media, Salt Lake City, Utah).

The offtake plate at the bottom of the column is grooved concentrically into eight evenly spaced collecting rings, as shown in Figure 8. Each groove except the innermost one is separated into three 120° sectors to permit testing for radial symmetry of solute bands. From the grooves the fractions flow through polyethylene tubing to a sample-collecting manifold, one element of which is shown in Figure 9. Glass-and-Teflon needle valves (Fisher Scientific Co.) and on-off valves (Hoke Mfg. Co.) allow fine control of the 23 offtake flows which are read on miniature rotameters. Rapid-response temperature probes (Cole-Parmer tissue implantation probes No. 8456) of 0.024-inch o.d. are inserted into several offtake lines, at the bed outlet, to allow measurement of the outlet temperatures that are developed and hence of the heat generated by electric-power dissipation.

Elutant solution enters through the clear Lucite acrylic-resin disk shown in Figure 10. Both the upstream fitting of Lucite (which offers a direct view of the top of the column) and the downstream offtake plate of Teflon (described above) have inlets or outlets for the electrode compartment coolant. The coolant streams flow concurrently with the elutant.

The solute feed enters the bed through one of three rings of Type-304 hypodermic needles (one ring is shown in Figure 10). The needles (of 0.042-inch o.d., 0.027 inch i.d., and 3.25-inch length) are silver-soldered into the annular manifold, and penetrate about 0.25 inch into the packing to prevent side mixing with elutant at the top of the bed. The needles and rings have been electrically insulated with Scotch-Weld structural adhesive. Each needle is pointed to provide a large elliptical port which opens in the tangential direction.

The coolant stream for the inner electrode enters above the top plate and exits below the offtake plate, through polyvinyl chloride tee fittings which also support the electrode. Connection of the inner electrode to the current source is made at the top of the column, by a copper sleeve clamped to the cable from the rectifier. The electrical connection for the outer electrode is made at the bottom of the Hastelloy screen, through a copper-plated rod extension, to another sleeve clamp.

By solution and entrainment, each coolant stream washes away any gas trapped between the respective diaphragm and electrode. In order to maintain a relatively large pressure drop in the outer coolant compartment, it is lined with plastic mesh screen and polyethylene sheeting. Coolant enters through two ports in the Lucite disk at 45° to the vertical (to reduce channeling) and exits through six ports in the Teflon offtake plate.

The Lucite disk for input elutant is held in a compression fit by an annular stainless-steel top plate (14.5 inches in diameter, 0.50 inch thick) which is bolted to a standard steel gasketed flange around the outside flared end of the exterior glass pipe. The entire separation unit rests upon a stainless-steel support plate (14.5 inch diameter, 0.75 inch thick) to which the lower glass-pipe flange is secured by a circle of bolts. Three 3/4-inch (nominal) supports or "legs" (16 inches high, 0.75 inch diameter) are threaded left-handedly to the support plate and also threaded to floor flanges to allow leveling the column.

Auxiliary Components

Most of the auxiliary pieces are indicated in the flowsheet, Figure 6: offtake sampling rack, power source, coolant storage drum, degasifier, valves and rotameters, and feed and elutant storage tanks.

Rotameters are used for metering the elutant, coolant, cooling water, and degasifier air supply. A positive-displacement pump (Lapp Microflow Pulsafeeder L5-20, used to regulate the feed flowrate) and centrifugal pumps (Eastman Industries E-1 for elutant and Worthington for coolant) are floor-mounted.

Manometer taps have been installed in the PVC piping to measure pressure differences between the bed and the two electrode compartments. Regulation of the unit is complicated by an appreciable permeability of the diaphragms, about 0.6 cc per hour per in^2 per foot of water-head. Gate valves in the coolant lines between the column and the degasifier allow adjustment of the coolant streams to the pressure level within the packed bed, so as to minimize transverse flow through the diaphragm.

Leaks can be detected between the bed and either coolant compartment by observing the pressure drop produced when the valves to the other compartment and also on the bed offtake are closed, and elutant is pumped into the bed; a pressure drop less than normal indicates a leak.

Temperature measurement of the elutant (upstream) and the inside coolant (upstream and downstream) are made by probes (Cole-Parmer no. 8444 tubular stainless steel, 5/32 inch diameter) inserted through the external piping.

Degasifier. Coolant flow rates, at a power input of 2 kw, set to keep the temperature rise within streams 1°C, are 3.5 for the inside stream and 11.5 gpm for the outside stream. The coolant streams leaving the column flow into separate sections of an aerated degasifier column 6 inches in diameter and 30 inches high, partly packed with 0.75-inch Raschig rings, to remove dissolved hydrogen (cathodic) and oxygen (anodic). For a maximum 50-amp current, in order to preclude an explosive level of hydrogen in air, the required aeration flow rate is 1 ft^3/min. Subsequently the streams are mixed for mutual neutralization of base (cathodic) and acid (anodic), and degasified remixed coolant drops into the 50-gallon storage tank where it is recooled. Throughout, the cooling system is built of unplasticized PVC pipe.

Power source. A voltage-regulated silicon rectifier (Rapid Electric Co., Bronx, N. Y.) has continuous-service maximum outputs of 50 volts and 100 amps.

Operating Experience

The experimental column has run for as long as 12 hours without operational difficulties. A manual is available describing the startup, running, and both normal and emergency shutdowns (Vermeulen and Tobias, 1964). In start-up operation, difficulties arose in maintaining desired pressure levels and flow rates, and in repairing leaks at various points in the separation unit. The column is first run without current, and with dye feed, until the operation in general and the offtake symmetry in particular are satisfactory. During a typical run, the pressures, flow rates, voltages, current, and temperatures can be recorded at half-hour intervals by a single operator.

RESULTS AND DISCUSSION

Temperature and Voltage Profiles

In general, experimental temperature profiles agree reasonably well with theoretical profiles predicted from the constant-property treatment. Figure 11 shows outlet-end temperature points for a typical run, with a calculated curve using the apparent average diaphragm temperature as the wall value.

An observed radial voltage profile is shown in Figure 12. The plot reflects the fact that in cylindrical geometry the potential E at any radius r (relative to the value at the outer diaphragm) varies linearly with $\ln r$. Consistent with Equation 6,

$$E = (i/2\pi k_m) \ln \frac{r_a}{r} \qquad (19)$$

where i is the total current per unit height of bed. From voltages measured at two feed rings relative to the outer electrode, and from electrical conductivities measured for the coolant, the voltage drops across the bed and coolant compartments can be calculated; the remaining voltage drop is attributed entirely to the diaphragms and is seen to be relatively large.

Radial Dispersion

Data for typical runs without current are plotted in Figure 13 on probability-linear coordinates, corresponding to the Gaussian relation of Equation 16. The indicator Apolon is a neutral dye (molecular weight 342, absorption peak at 440 mμ) which is useful in studies of electroosmotic effects in electrophoresis. Agreement with the predictions for the rectangular model is quite good, even for the inner feed ring. (The agreement is poorer for electrophoretic runs, as discussed below, mainly because of operating difficulties.)

Separations

To explore the separation capacities of the continuous electrophoretic apparatus, inexpensive, readily analyzed compounds have been used in the feed mixtures. Binary mixtures of dyes and of amino acids have received the greatest attention. The dyes studied, with properties reported by Werum *et al*. (1960), were Apolon (neutral), Brilliant Blue (-2), and Amaranth (-3); the amino acids used were glycine, glutamic acid, lysine, asparagine, and proline. The analytical techniques employed were direct spectrophotometry for the dyes; the ninhydrin spectrophotometric method for most amino acids, as given by Greenstein and Winitz (1961); and polarimetric detection for proline.

Amaranth-Brilliant Blue. Because dyes give immediate visual evidence of degree of separation in experimental runs, Amaranth and Brilliant Blue were used extensively in characterizing the unit and developing operating control. A block offtake pattern for the separation of this dye pair is shown in Figure 14. In this case the peaks of Amaranth (three negative charges) and Brilliant Blue (two negative charges) occur in rings 2 and 4, respectively. This run indicates that species with any greater difference in ionic charge should separate extremely well.

Glycine-Glutamic Acid. The first attempted amino acid separation was performed on the pair glycine-glutamic acid. Since the ninhydrin spectrophotometric analysis cannot distinguish between amino acids, the movement of each component in the column was first studied separately. Offtake-patterns for these runs are shown in Figure 15. At the pH of these experiments, approximately 7.0, glutamic acid has one negative charge while glycine is neutral. In this case the peaks of the amino acids are separated by two rings, with nearly 40% of the glutamic acid in ring 3 and over 40% of the glycine in ring 5. Subsequently, a run was made with a mixed feed of the two components. The combined offtake patterns, Figure 16, indicates that the separation was even better than that predicted from the separate runs.

Asparagine-Proline. The most sensitive test of the separation capabilities of the unit to date involved a mixture of the amino acids asparagine and proline. Compared to entirely anionic glutamic acid with neutral glycine (at pH 6.9), the asparagine at pH 9.3 was 75% in anionic form, and the proline was 5% in anionic form; thus the latter mixture is more difficult to separate. In a run with mixed feed at pH 9.3, polarimetric detection of L-proline in the offtake samples made it possible to establish separate offtake patterns for the two solutes. The block offtake pattern in Figure 17 indicates a fairly clean separation, even though asparagine has overlapped into ring 8. Channeling within the bed, slight imperfections in the offtake-plate gasketing, and imperfect control of offtake flow rates may all contribute to the observed distortion of the offtake patterns. In general, however, over 90% of a solute band appears within three offtake rings.

Conclusion

The separations just described demonstrate the practicality and predictability of using continuous electrophoresis for solute feed rates of 100 to 1000 grams per hour. The problem of collecting fully separated fractions favors a larger radial thickness of bed, while the need to restrict the temperature rise limits this thickness. Thus, units giving even larger production rates will still require thicknesses of 5 to 10 cm. Cylindrical units larger than the present one will require a lower curvature and will tend toward rectangular geometry.

Better operation and performance would be obtained if diaphragms were developed that would give lower rates of electro-osmotic transport, but were unchanged or enhanced in their electrolytic conductivity.

ACKNOWLEDGMENT

The authors express their appreciation to Ray M. Hybarger for the initial design of the system; to Victor S. Engleman, M. Amin Mandil, Virendra N. Gupta, William Clewell, and Clark Edson, for assistance in assembling and operating the apparatus; to Michael C. Kavanaugh, Frank Pan, Michel Masson, and Peter N. Tenney for help on numerical computations; to Kwang-Lo Tsang and Allan Champion for studies of radial dispersion; to David R. Buss and Rolf Muller for valued counsel; and to Charles W. Tobias for his collaboration in launching this project.

NOMENCLATURE

A'	Coefficient
C	Normality of solute at a point (g-equiv./ℓ.)
C_o	Normality of solute in feed (g-equiv./ℓ.)
C_m	Maximum normality at the offtake (g-equiv./ℓ.)
c_p	Specific heat capacity of elutant at constant pressure (watt/g°C)
d_p	Packing particle diameter (cm)
D_r	Total radial diffusivity (cm^2/sec)
E	Electrical potential (volt)
E_{ab}	Electrical potential across bed (volt)
E'	Reduced electrical potential (= E/E_{ab})
i	Current density (amp/cm^2)
J_o	Bessel function of zero order, first kind
j	Integer subscript, order of eigenvalue
k_h	Effective thermal conductivity of bed (watt/cm°C)
k_m	Effective electrical conductivity of bed (mho/cm)
L	Total length (or effective length)
P	Production rate (g-equiv./sec)
Q	Temperature rise coordinate (= $k_m(E_{ab}/\ln r_o')^2$) (watt/cm)
q	Strength of feed (g-equiv./cm sec)
r	Radial coordinate (cm)
r_a	Radial position of outer diaphragm (cm)
r_b	Radial position of inner diaphragm (cm)
r_F	Radial position of feed ring (cm)
r_L	Radial position of solute peak at the offtake (cm)

r_p	Radial position where $T = T_p$ (cm)
r'	Dimensionless radial coordinate (= r/r_b)
r'_o	Dimensionless radial coordinate (= r_a/r_b)
s	Width of solute band at offtake (cm)
T	Temperature (^oC)
T_o	Temperature of coolant and of entering elutant (^oC)
T'	Relative temperature (= $T - T_o$)
T_p	Peak bed temperature (^oC)
T'_p	Relative temperature (= $T_p - T_o$)
t	Time (sec)
U_r	Linear velocity in radial direction (cm/sec)
U	Linear velocity in axial direction of elutant (= superficial velocity/cross-sectional area of bed) (cm/sec)
u	Effective electrophoretic mobility of solute (cm^2/volt sec)
Y_o	Bessel function of zero order, second kind
y	Axial coordinate (cm)
α_h	Thermal diffusivity (= k_h/ c_p)(cm^2/sec)
κ	Ratio (= k_m/k_h)(mho ^oC/watt)
λ	Eigenvalue
Φ	Function of eigenvalues
θ	Dimensionless temperature rise coordinate (= T'/ E^2_{ab})
θ_p	Dimensionless temperature rise coordinate for which $T = T_p$
ρ	Density of elutant (g/cm^3)
τ	Residence time in bed (= L/U_y)(sec)

LITERATURE CITED

Dobry, R., Finn, R. K., Chem. Eng. Prog. **54**, 59 (1958).

Finn, R. K., in "New Chemical Engineering Separation Techniques," H. M. Schoen, Ed., Interscience, New York, N. Y., 1962, Chapter 6.

Greenstein, J. P., Winitz, M., "Chemistry of the Amino Acids," Vol. 2, Wiley, New York, 1961, p. 1309.

Howery, D. G., Vermeulen, T., Birmingham Chem. Engr. **15**, 72 (1964).

Hybarger, R., Tobias, C. W., Vermeulen, T., Ind. Eng. Chem., Process Des. Develop., **2**, 65 (1963).

Masson, M., Kavanaugh, M., unpublished data, 1965.

Morris, C. J. O. R., Morris, P., "Separation Methods in Biochemistry," Interscience, New York, 1963.

Nady, L., unpublished data, 1965.

Porath, J., Ark. Kemi, **11**, 161 (1957).

Pucar, Z., in "Chromatographic Reviews," Vol. 3, M. Lederer, Ed., Elsevier, Amsterdam, 1961, p. 38.

Ravoo, E., Gellings, P. J., Vermeulen, T., Anal. Chim. Acta, **38**, 219 (1967).

Schoen, H. M., Ed., "New Chemical Engineering Separation Techniques," Interscience, New York, 1962.

Vermeulen, T., Tobias, C. W., "Annular-Bed Electrochromatography," Report 1 on Natl. Insts. of Health grant GM-08042 (1962).

Vermeulen, T., Tobias, C. W., "Annular-Bed Electrochromatography," Report 2 on Natl. Insts. of Health grant GM-08042 (1963).

Vermeulen, T., Tobias, C. W., "Annular-Bed Electrochromatography," Report 3 on Natl. Insts. of Health grant GM-08042 (1964).

Vermeulen, T., Tobias, C. W.,"Annular-Bed Electrochromatography," Report 4 on Natl. Insts. of Health grant GM-08042 (1965).

Vermeulen, T., Tobias, C. W., "Annular-Bed Electrochromatography," Report 5 on Natl. Insts. of Health grant GM-08042 (1966).

Werum, L. N., Gordon, H. T., Thornburg, W., J. Chromatogr., 3, 125 (1960).

Initial phases of the work described were performed under the sponsorship of the National Institute of General Medical Sciences, United States Public Health Service, through Research Grant GM-08042. Later phases were done under the auspices of the United States Atomic Energy Commission.

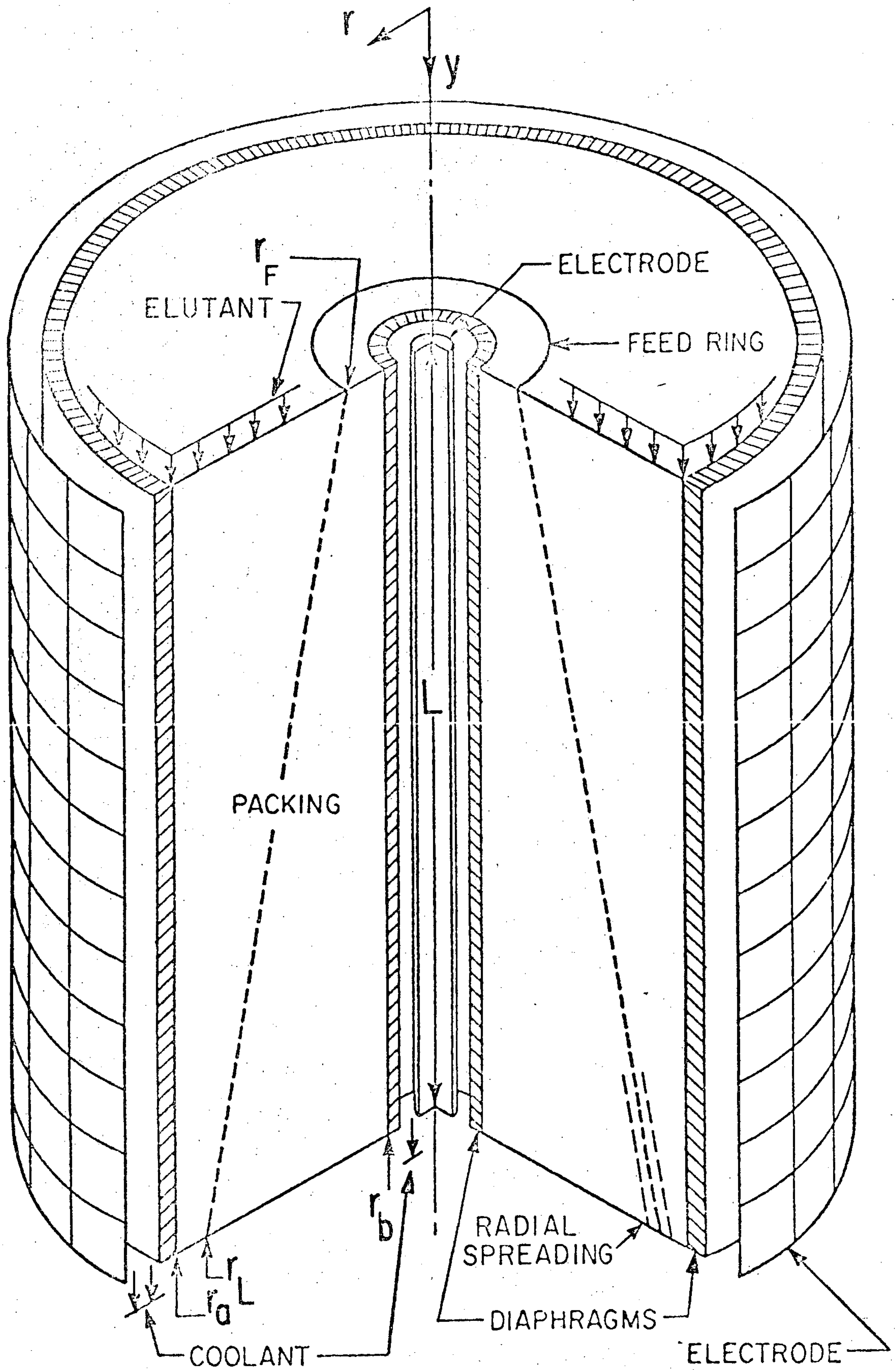

Figure 1. Sectional diagram of cylindrical column for continuous electrophoretic separation.

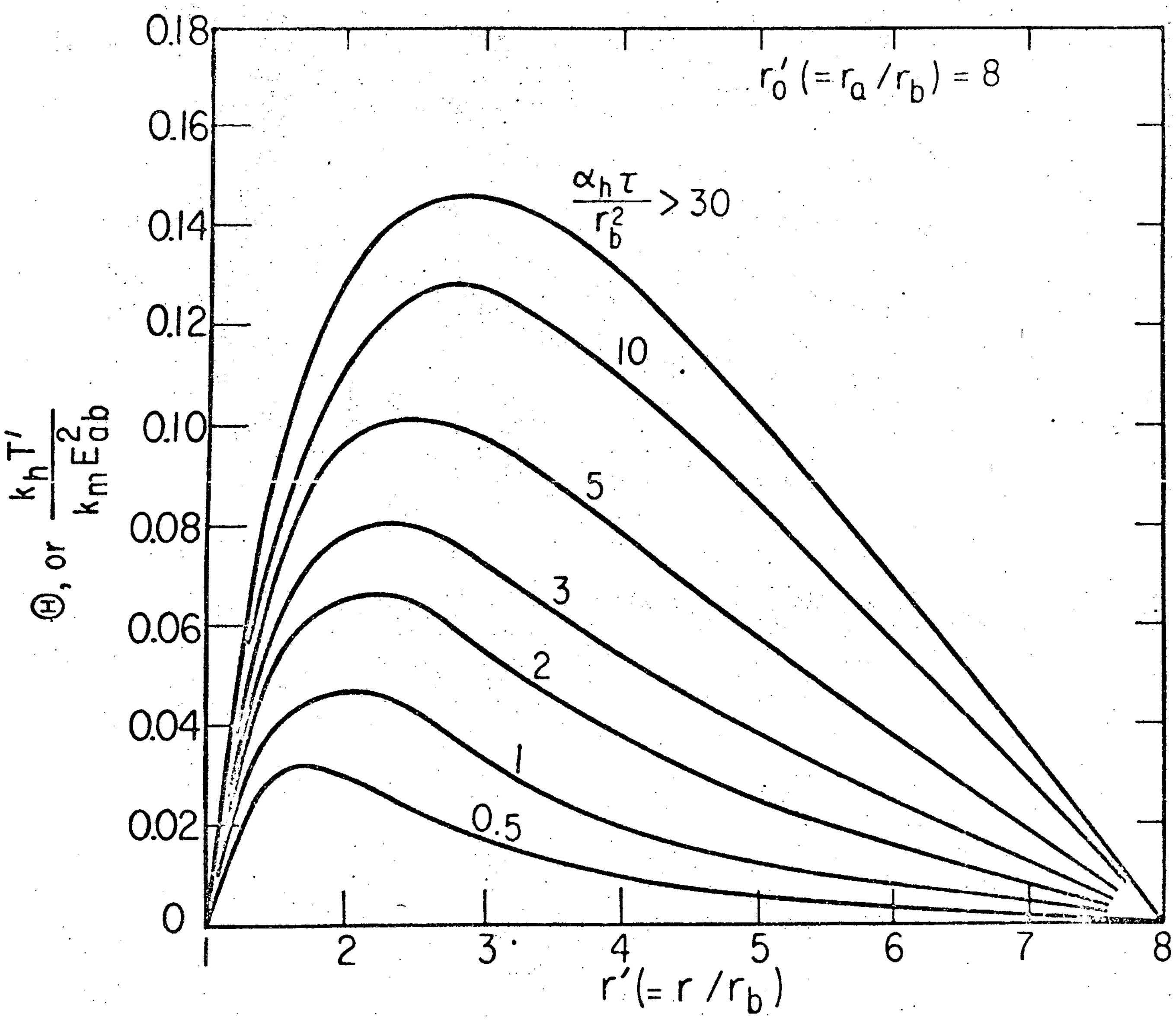

Figure 2. Profiles of residence-time group as a function of temperature-rise group and radial position, for $r_a/r_b = 8$.

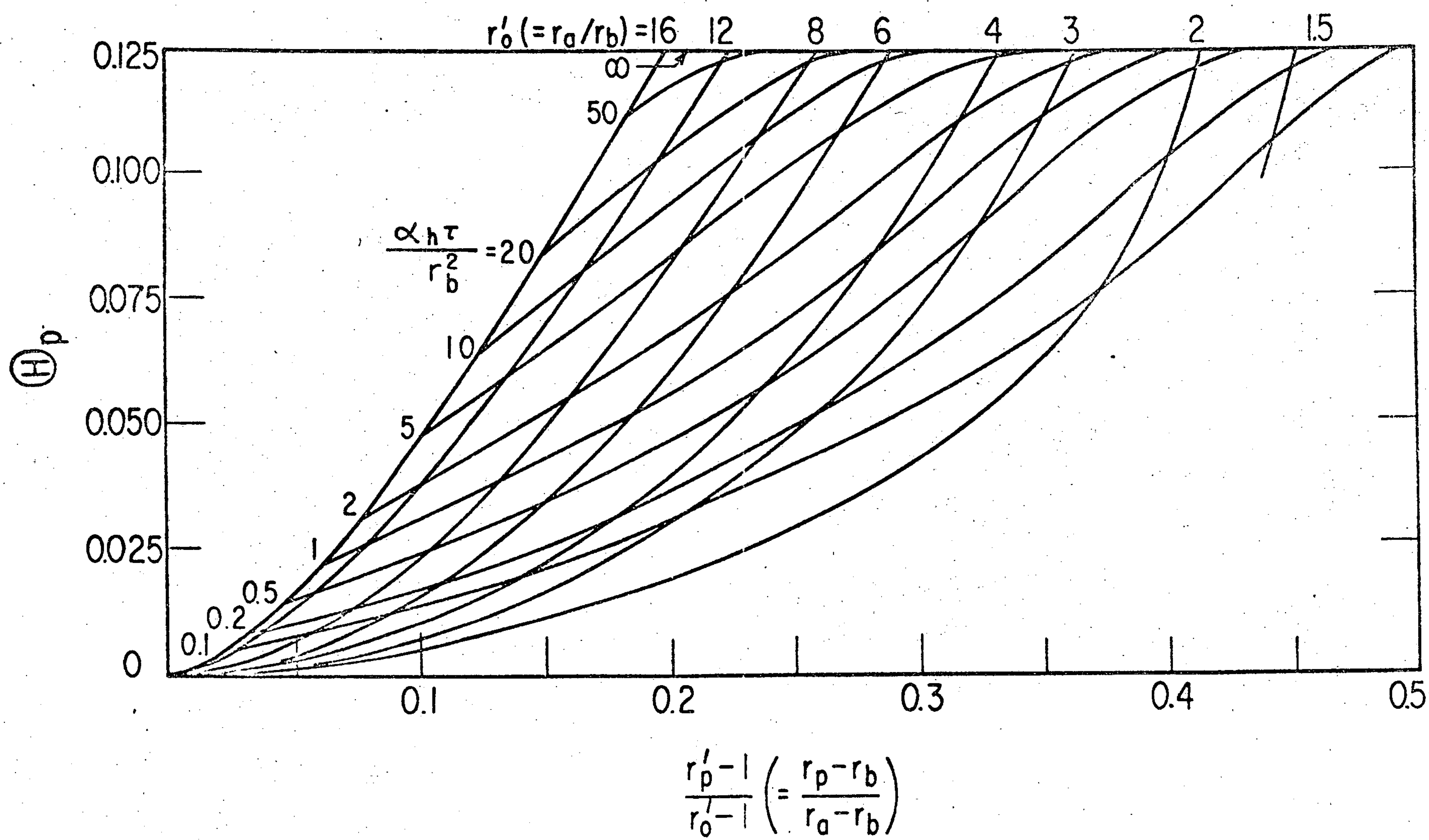

Figure 3a. Radial location of peak temperature, as a function of radius ratio, temperature-rise group, and residence-time group.

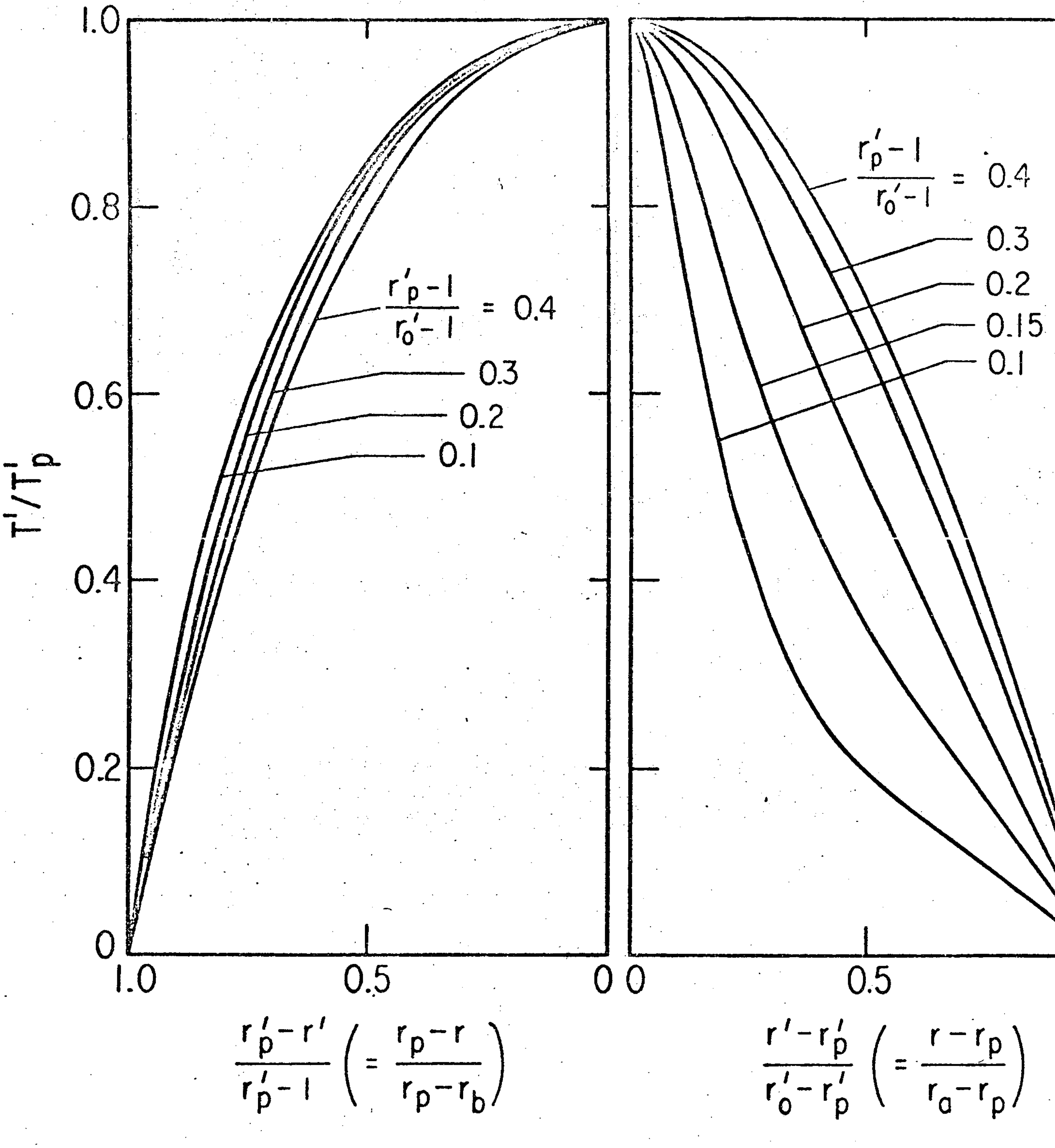

Figure 3b. Profile of temperature-rise ratio as a function of relative radial position and of peak-temperature radial position as given by Figure 3a.

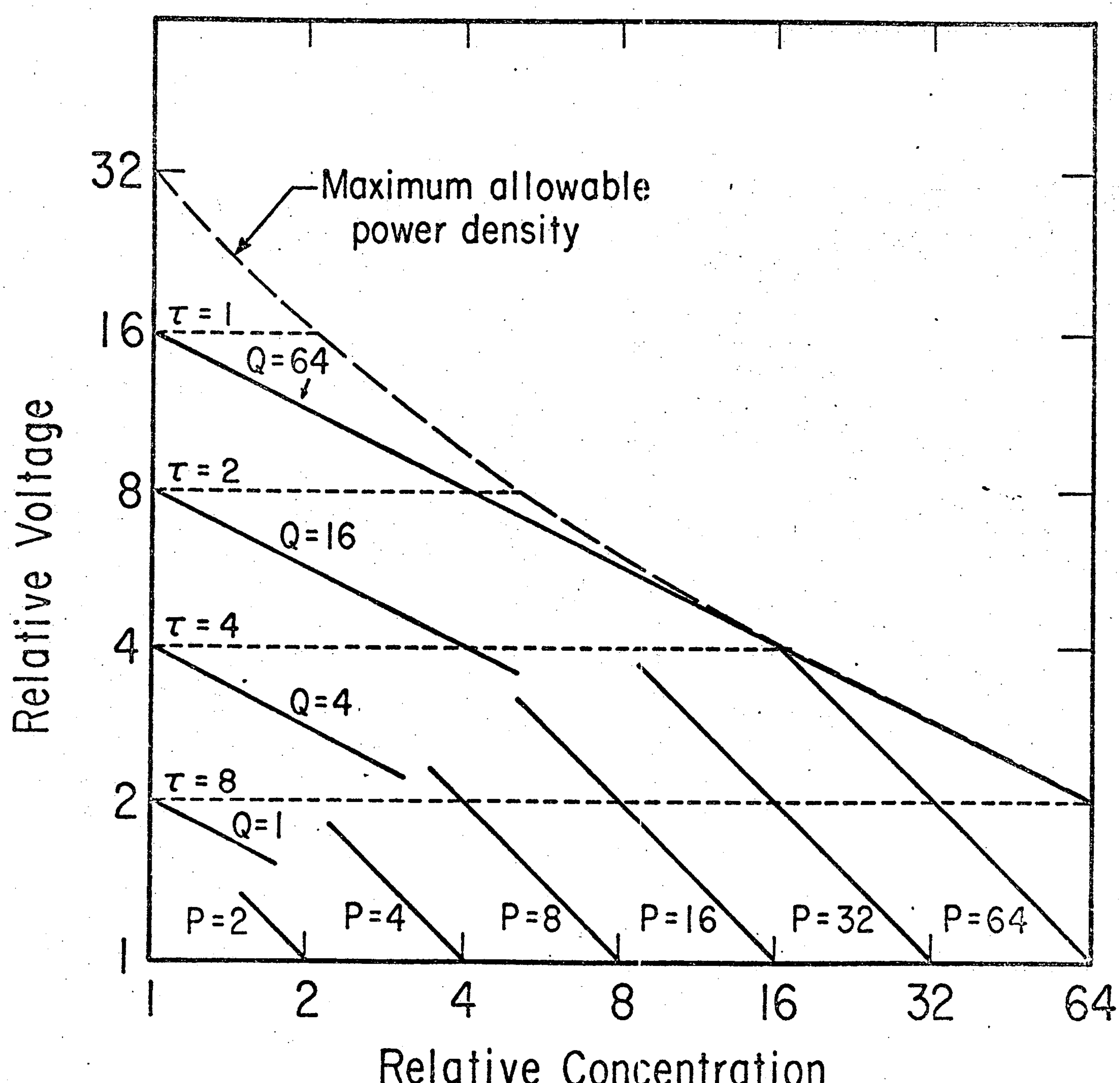

Figure 4. Schematic representation of relative operating voltage E and relative residence time τ needed to maximize the production rate P in a given apparatus, corresponding to restrictions of maximum allowable temperature rise or power density Q (— — —) and allowable concentration.

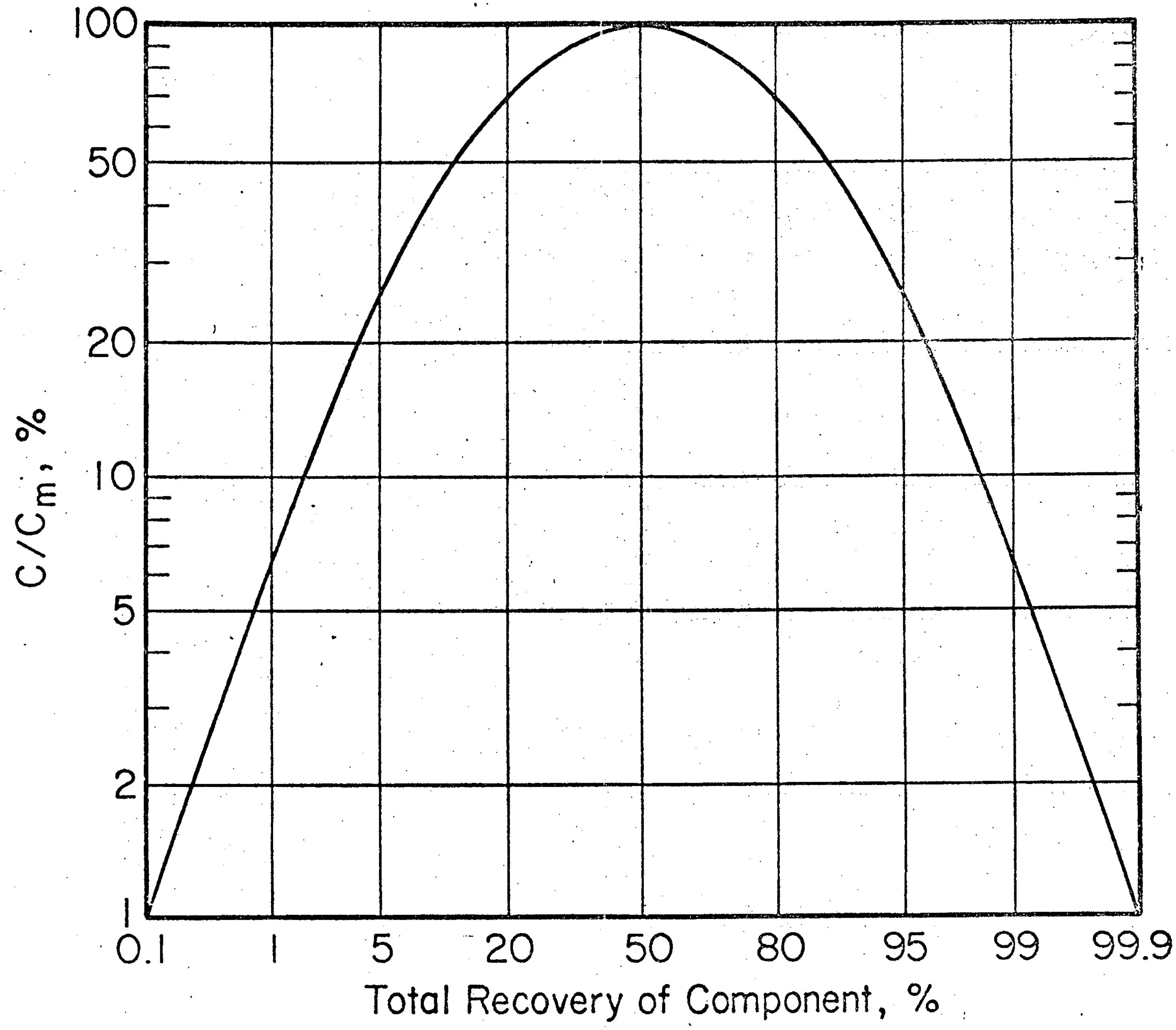

Figure 5. Relation between local solute concentration and integral recovery, for a solute band conforming to Gaussian distribution.

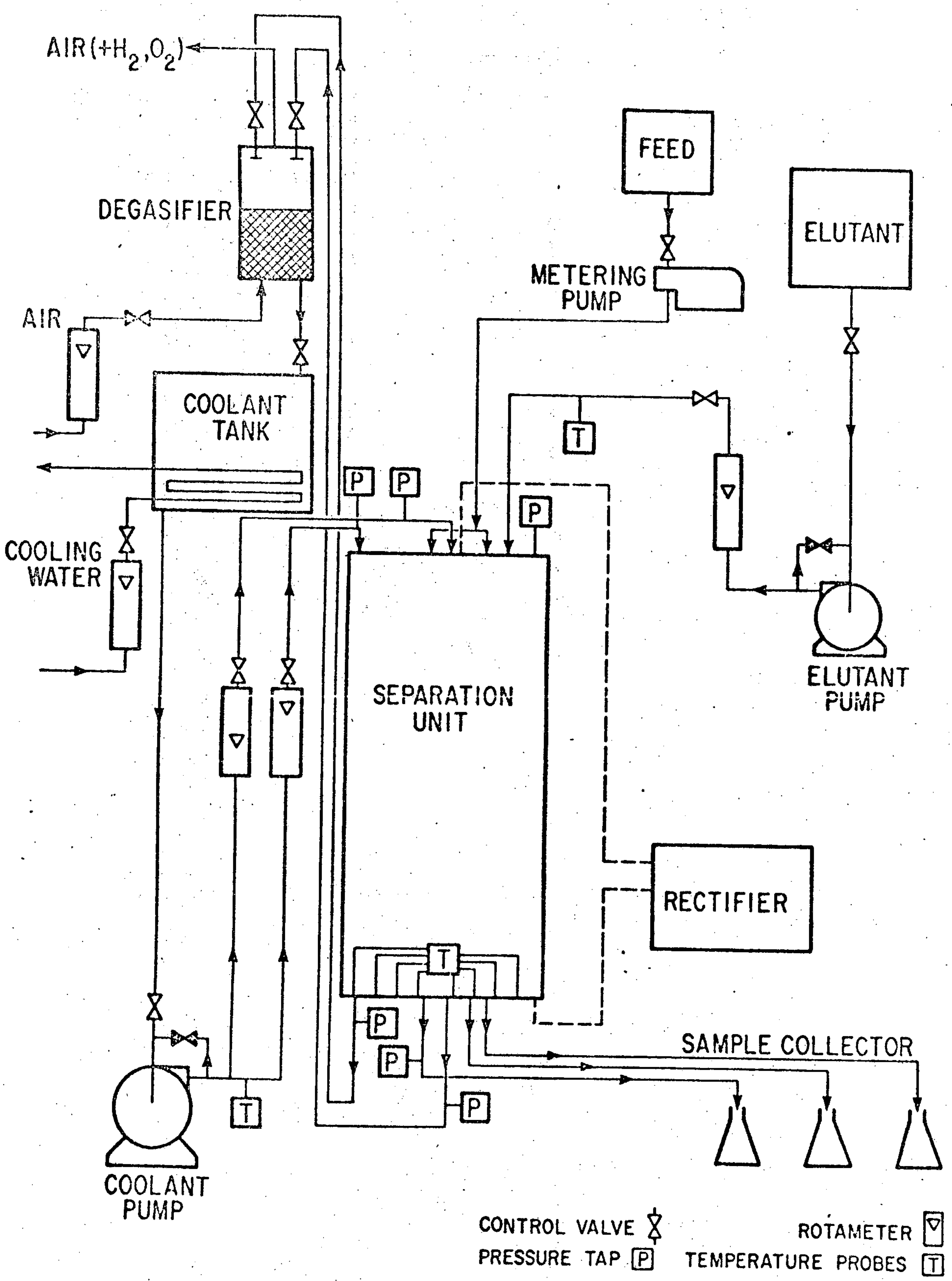

Figure 6. Flow diagram showing separation unit in relation to accessory equipment.

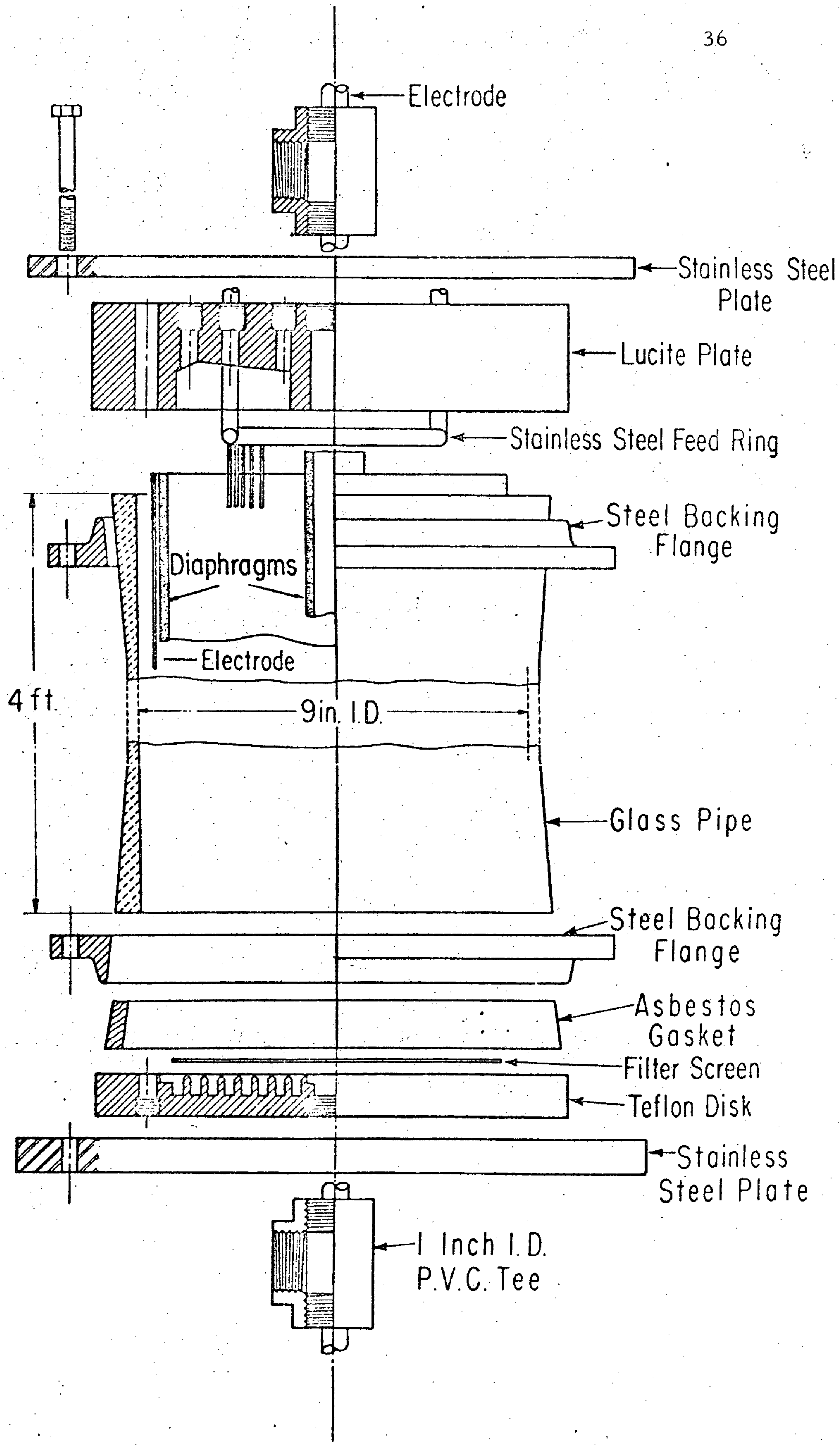

Figure 7. Exploded cross-sectional diagram of separation unit, showing construction and mode of assembly

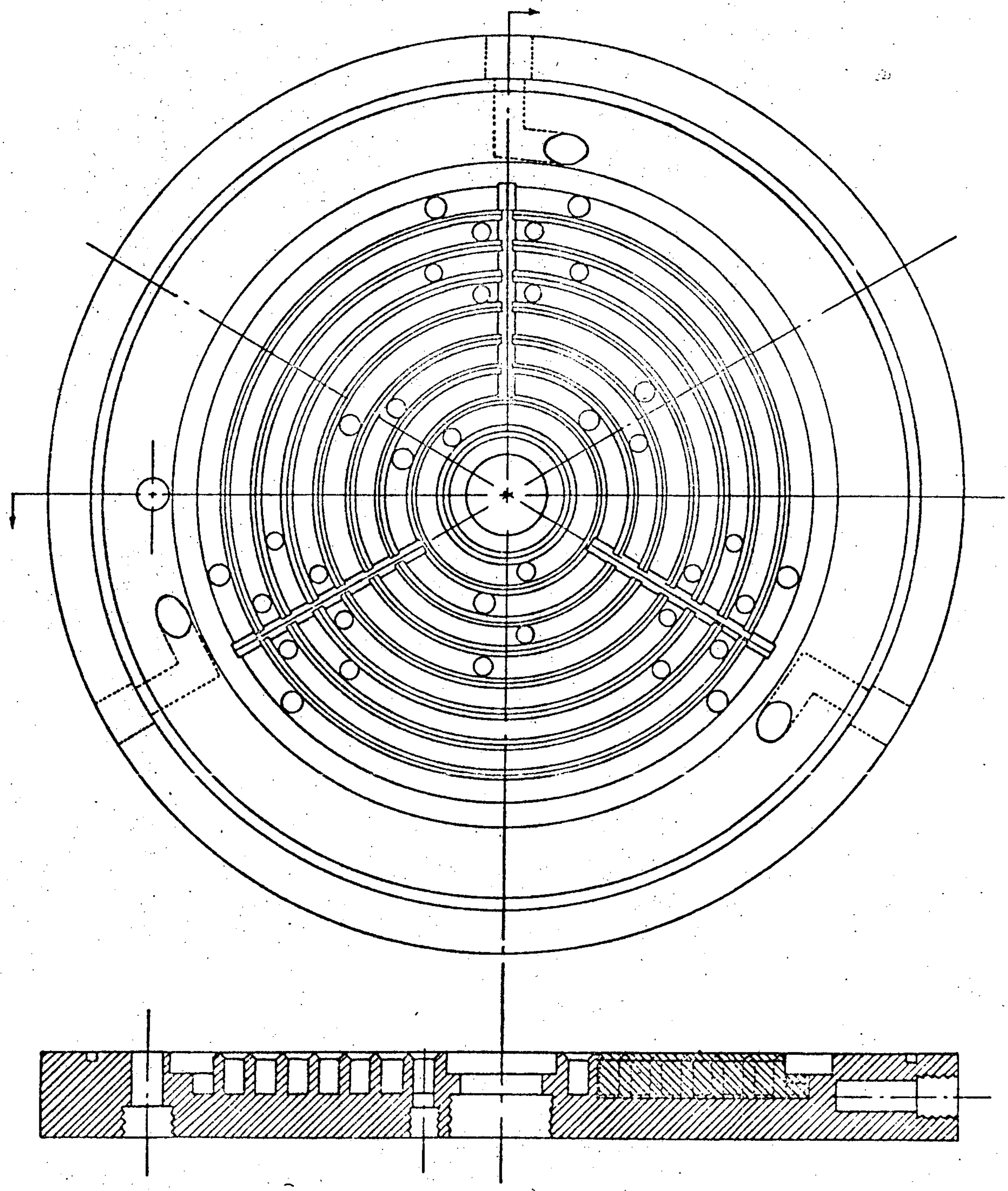

Figure 8. Radially compartmented offtake plate for separation unit. Dark circles indicate locations of thermister probes.

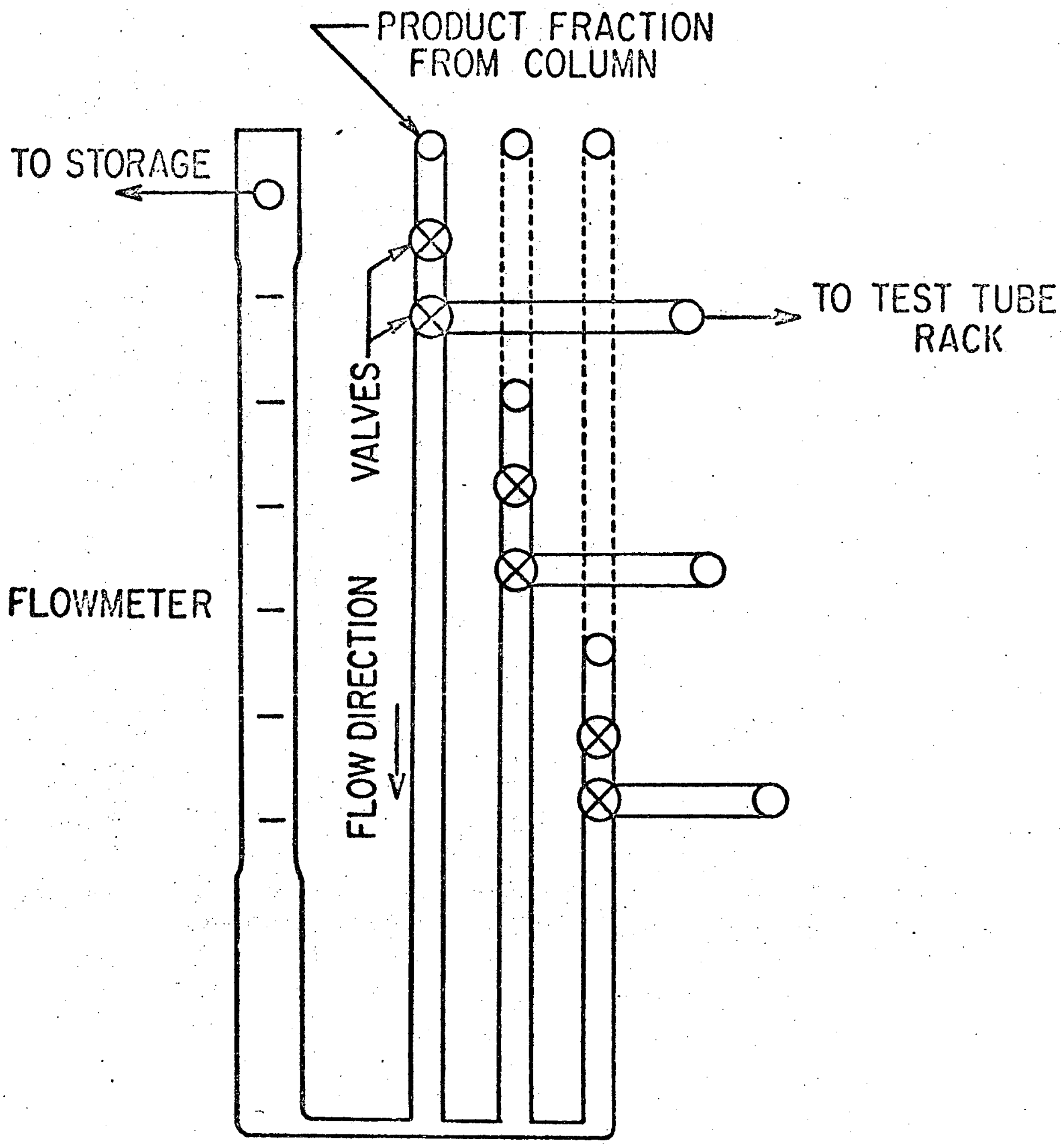

Figure 9. Arrangement of rotameter and valves for one modular section of the sample collector.

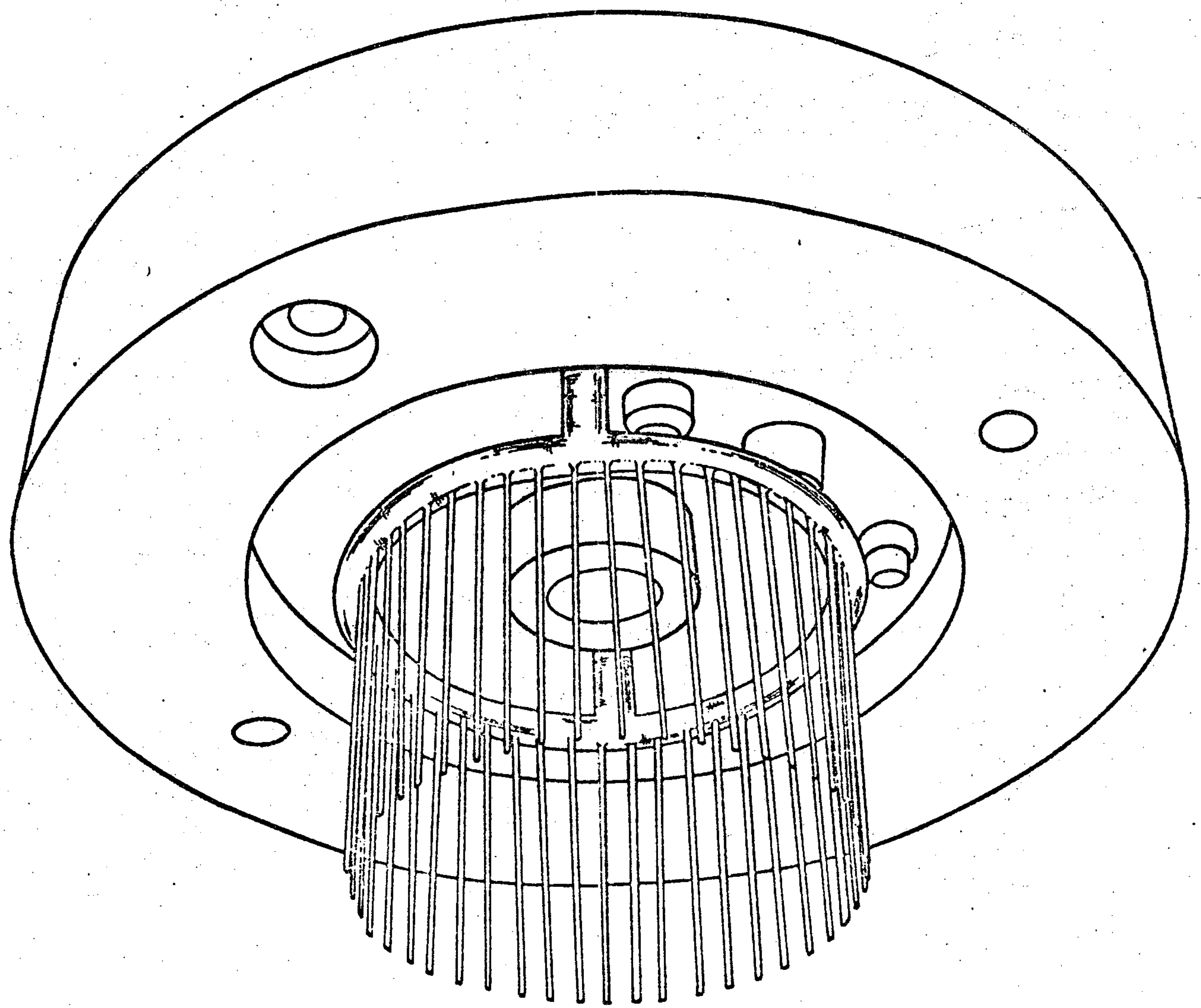

Figure 10. Lucite top plate and middle feed ring, showing feed tubes.

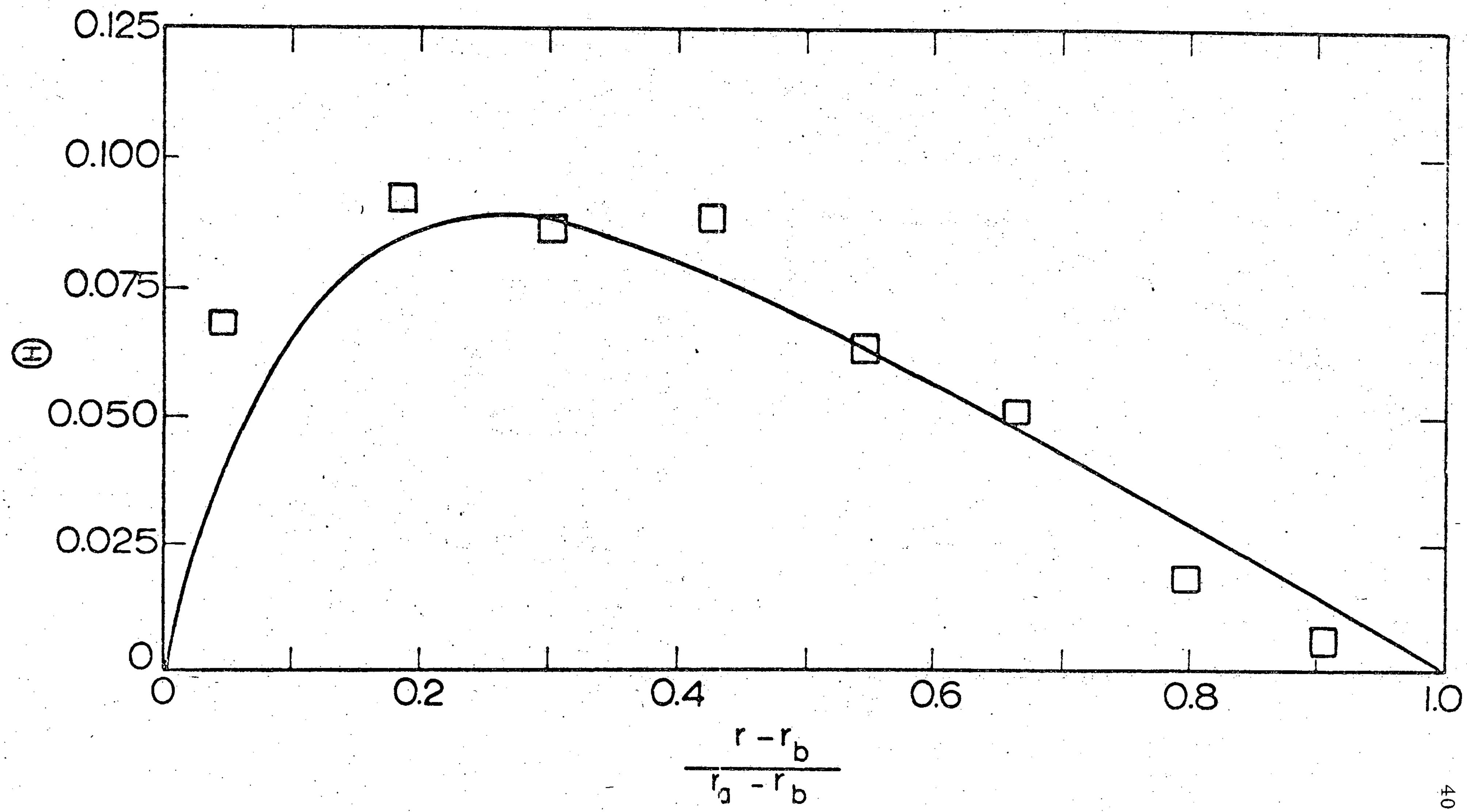

Figure 11. Experimental data for temperature-rise group, compared with theoretical profile, adjusted for heating of diaphragm. Radius ratio between diaphragms, 5.6; residence time, 2 hr.; voltage across bed, 13.7 V.; current, 18 amps.

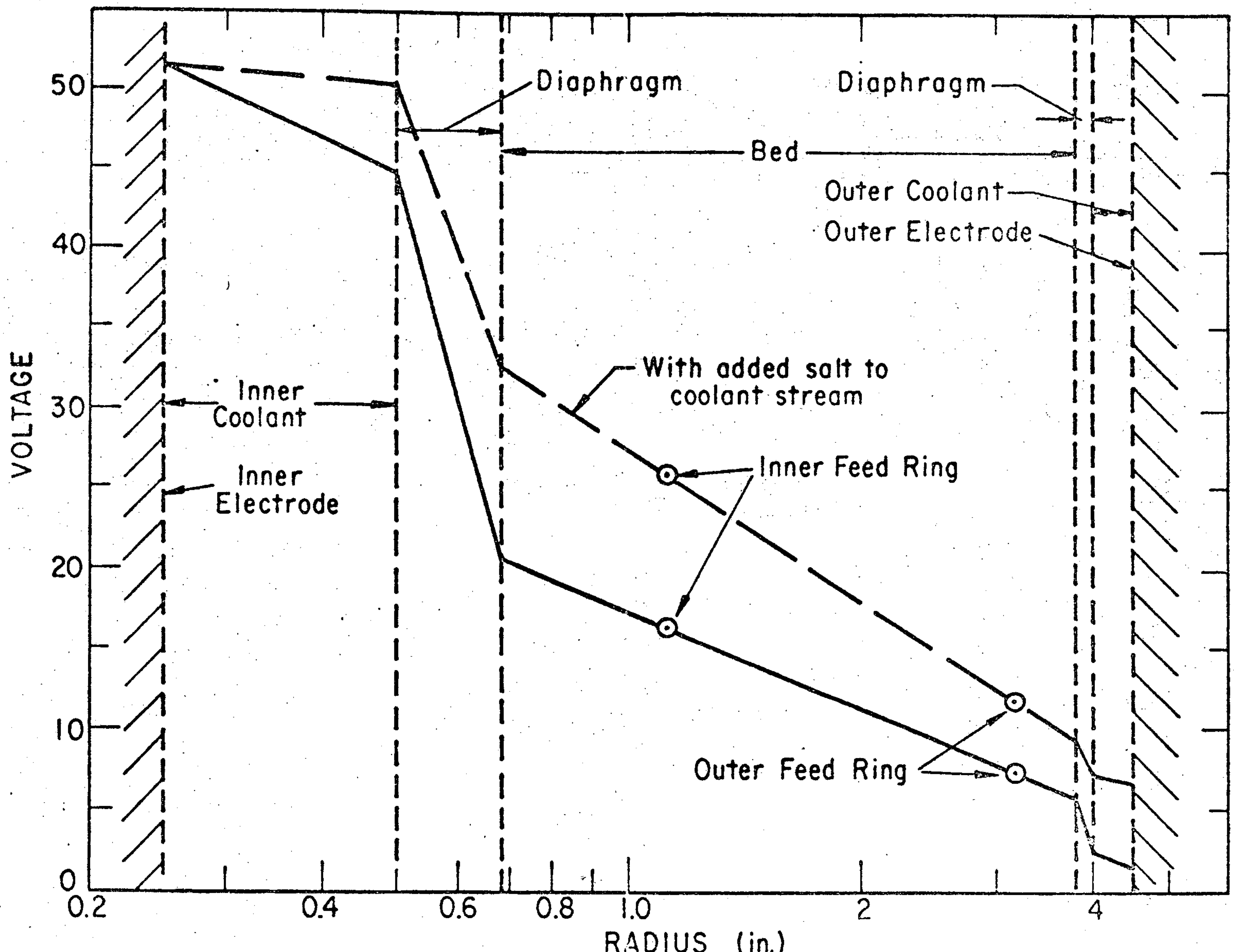

Figure 12. Experimental voltage profile; radius plotted on logarithmic scale. Elutant, 0.010M $NaNO_3$. Solid curve is for 0.010M $NaNO_3$ coolant; dashed curve for 0.090M.

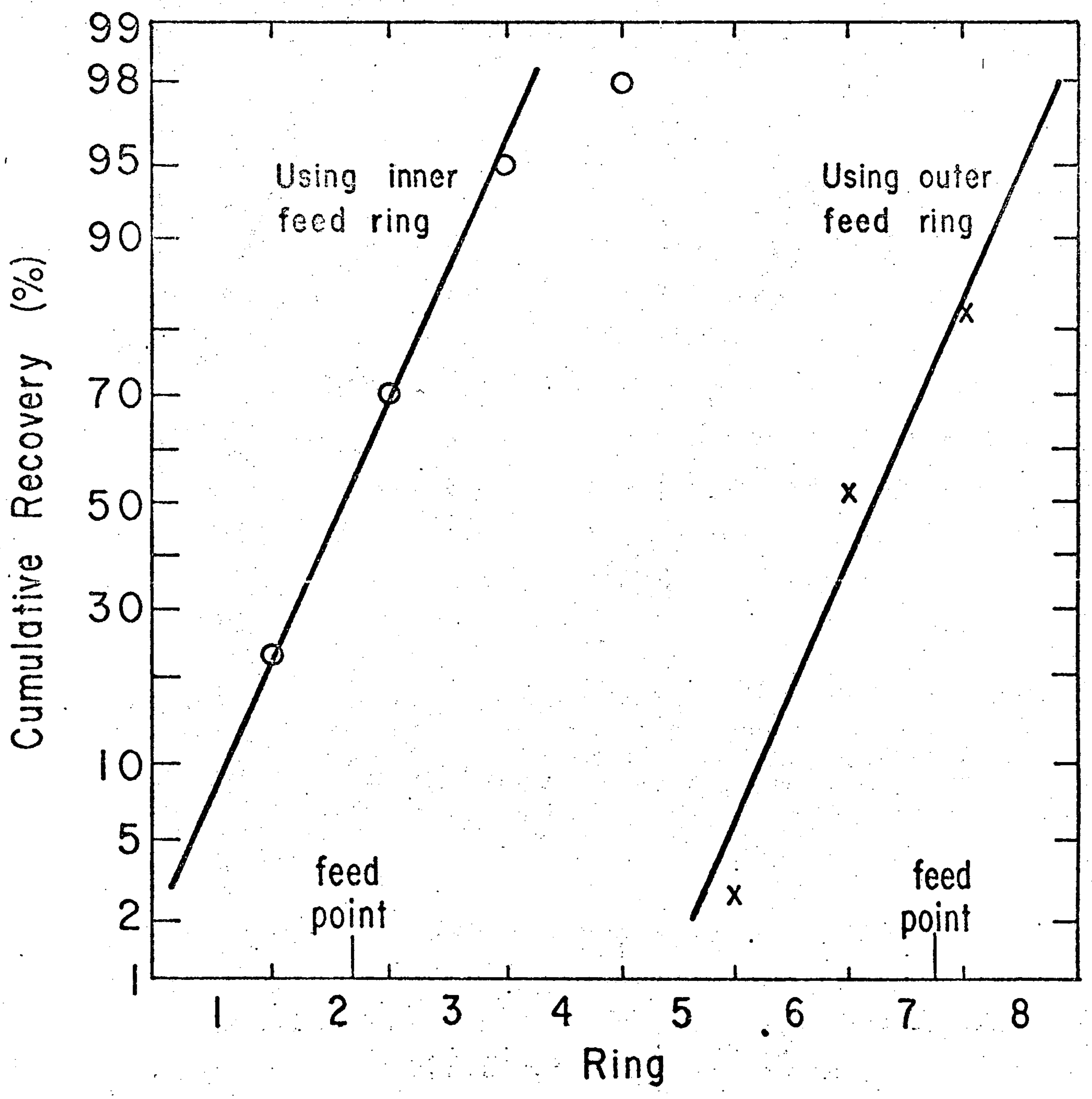

Figure 13. Radial dispersion of Apolon in column, without electromigration. Experimental points, with theoretical lines adjusted to experimental center of mass. Feed 0.5 ℓ./hr, elutant 7.0 ℓ./hr. Packing, 80-150 mesh polystyrene.

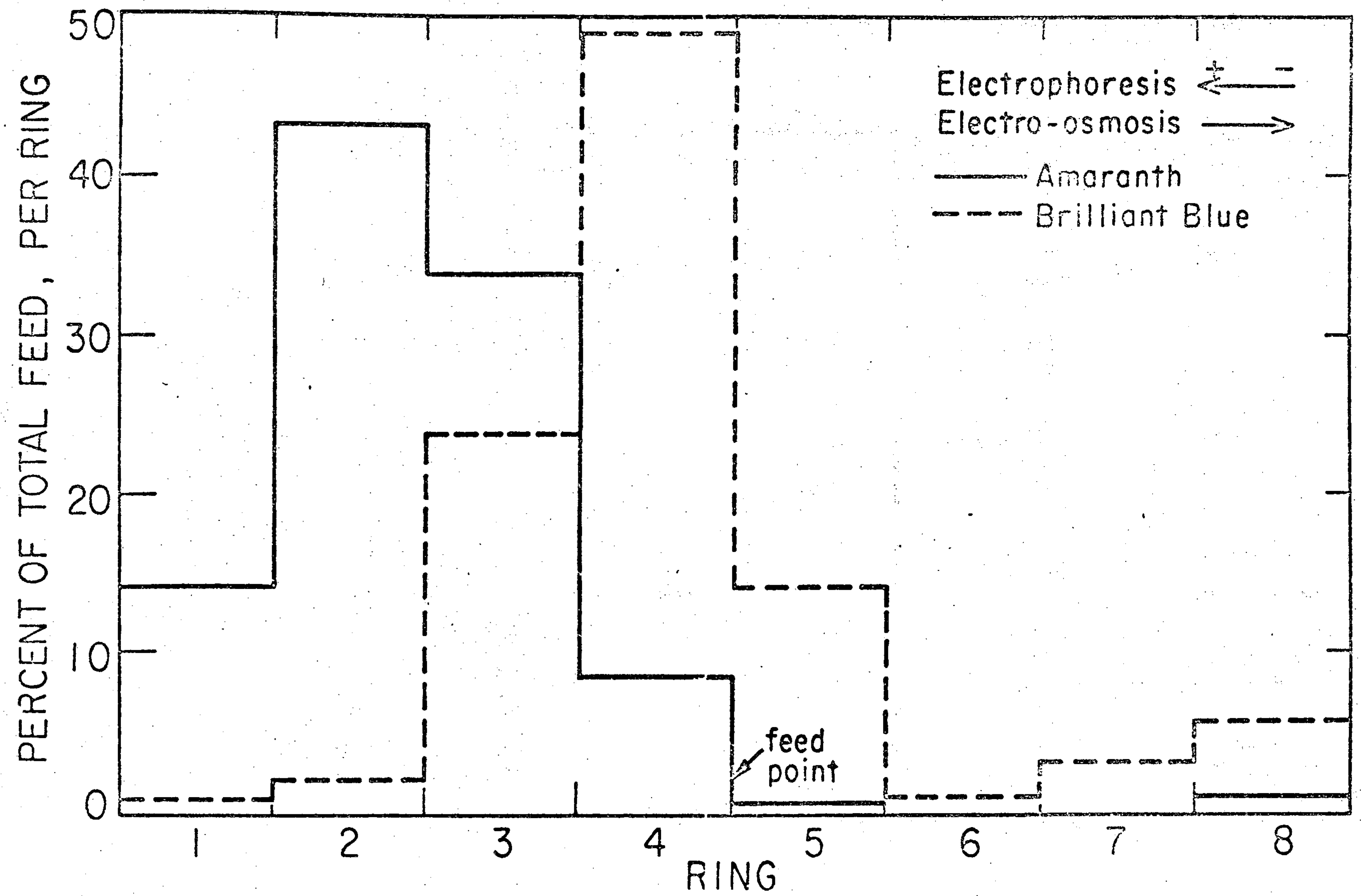

Figure 14. Experimental offtake pattern for Brilliant Blue-Amaranth separation trial in cylindrical column. Applied voltage 30 volts; residence time 2 hours. Elutant phosphate buffer (pH 6.9).

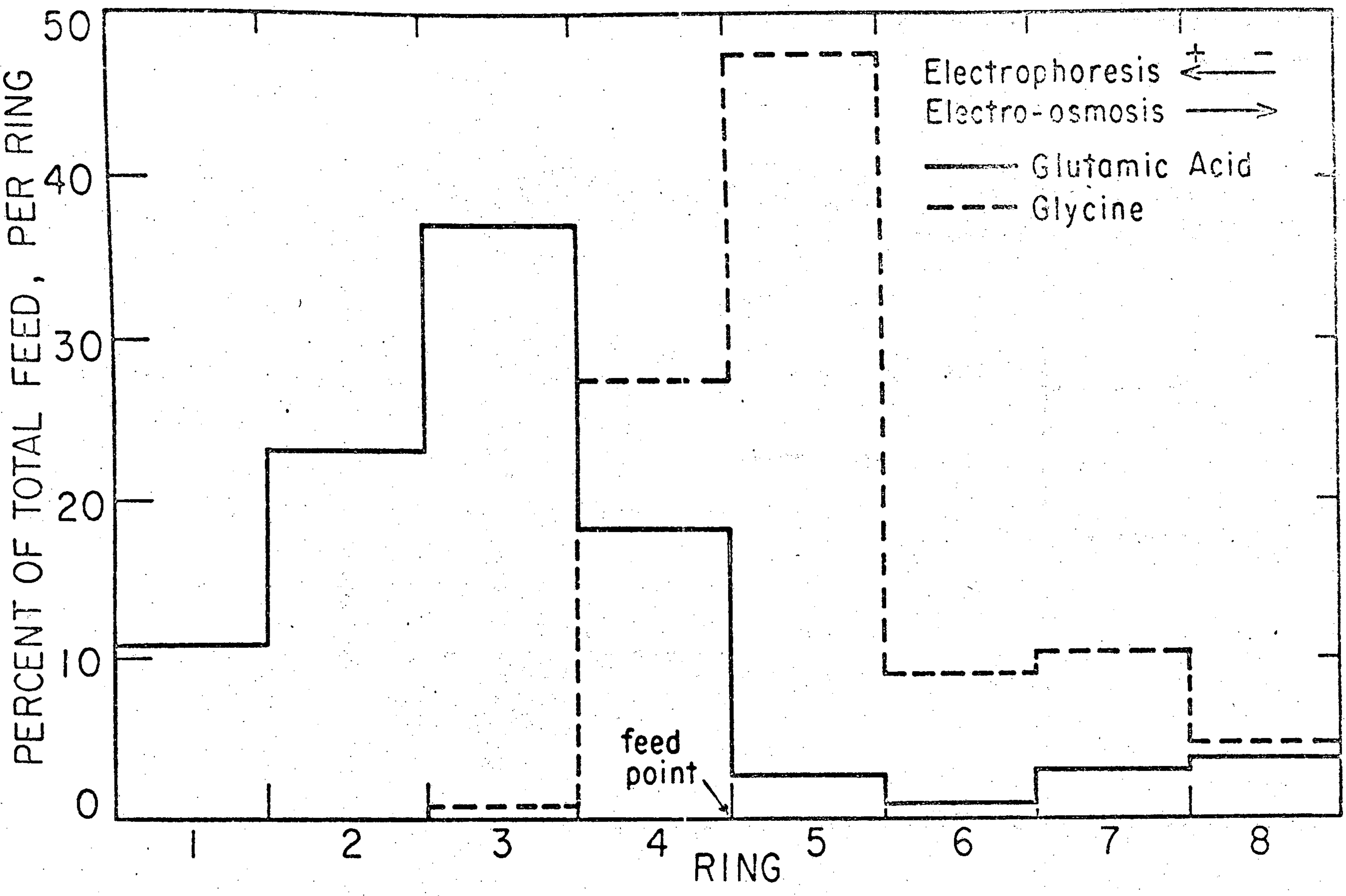

Figure 15. Experimental offtake patterns for glutamic acid and glycine run separately on the cylindrical column. Applied voltage 45 volts; bed voltage 16 volts; residence time 2 hours. Elutant, phosphate buffer (pH 6.9).

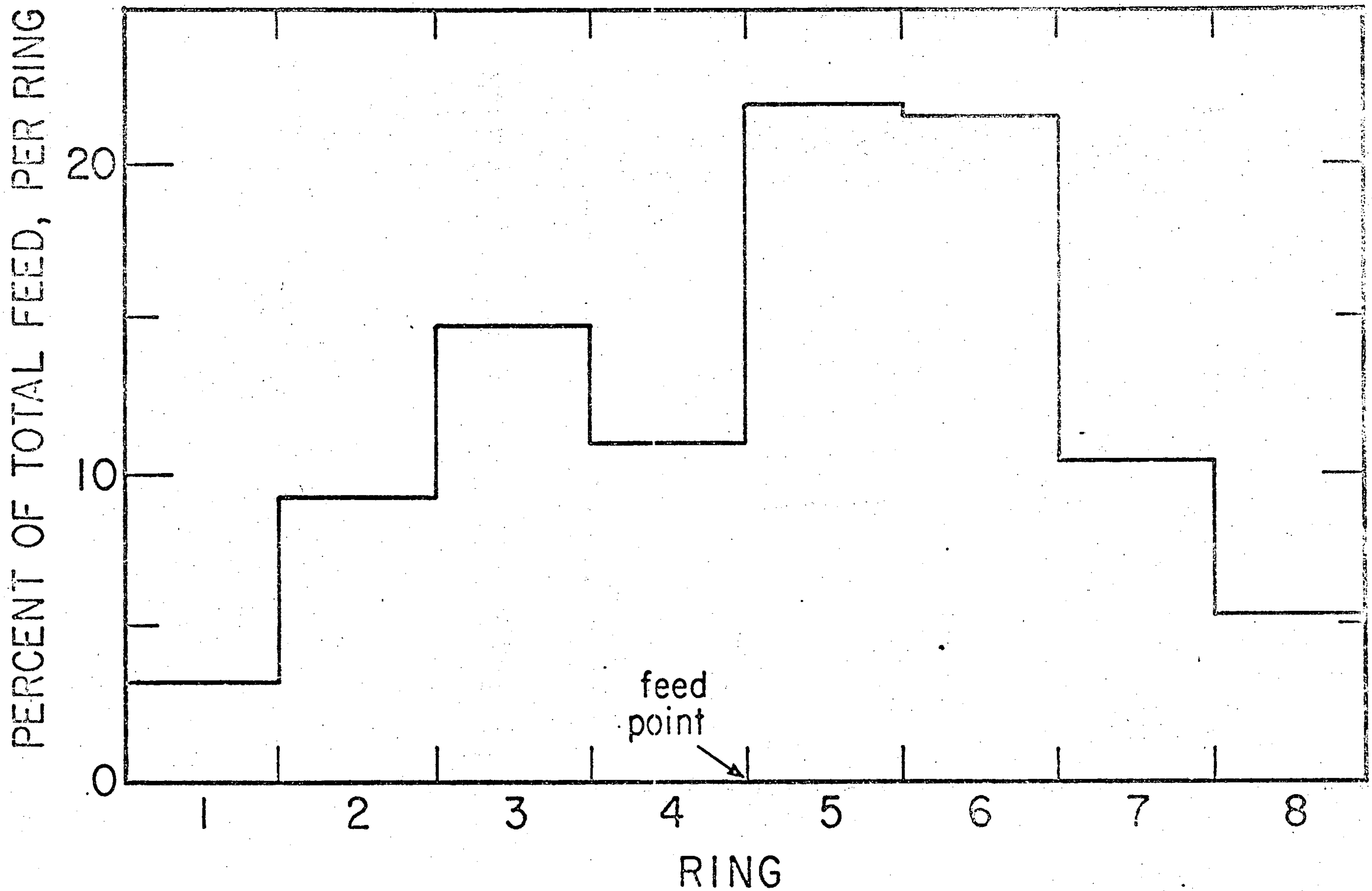

Figure 16. Experimental offtake pattern for glutamic acid and glycine fed together. Conditions same as for Figure 15.

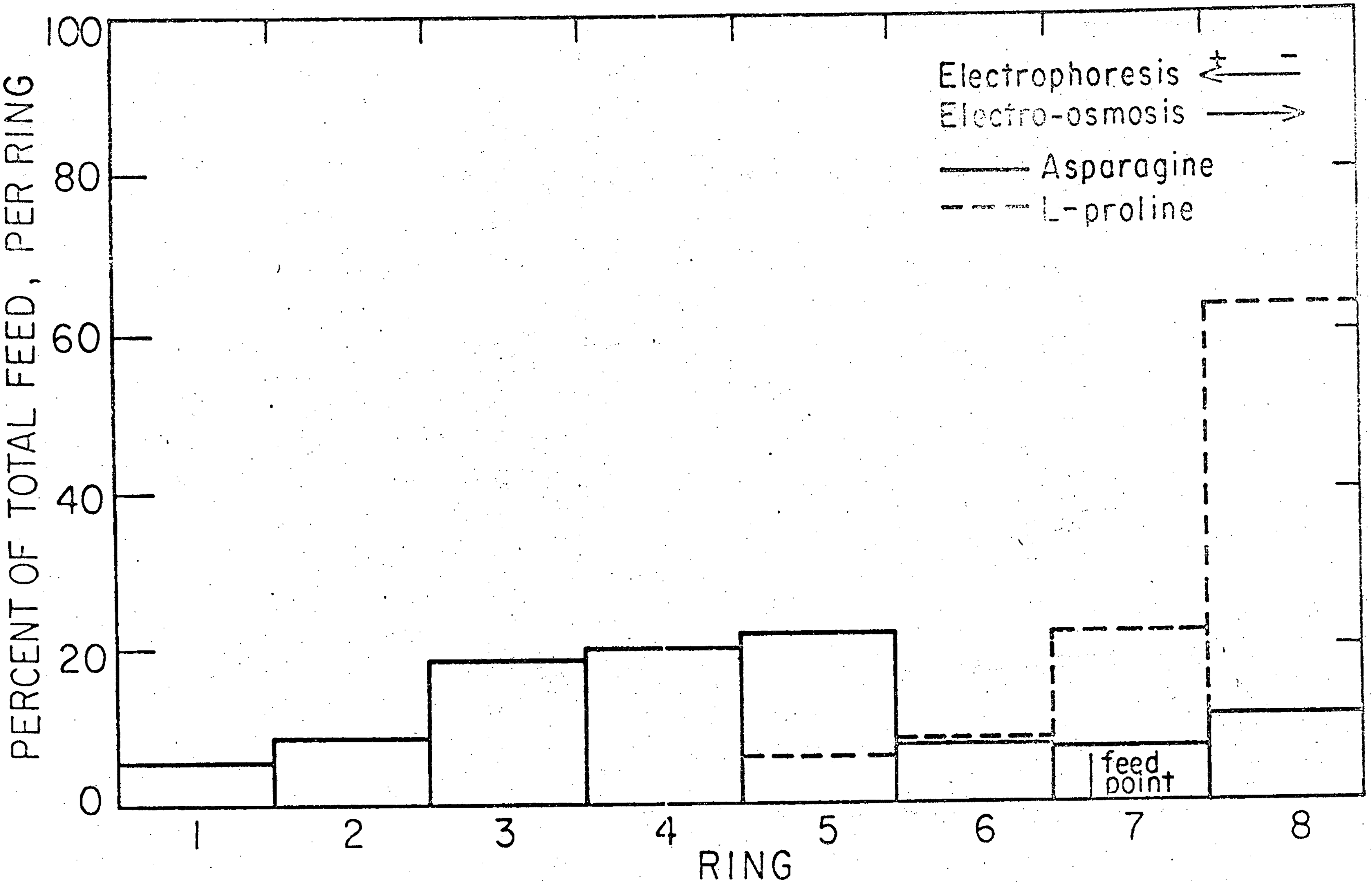

Figure 17. Experimental average offtake pattern for asparagine-L-proline separation trial. Applied voltage 50 volts; bed voltage 13 volts. Residence time 4 hours. Elutant, piperazine + trichloroacetic acid (pH 9.3).

TECHNICAL INFORMATION DIVISION
LAWRENCE RADIATION LABORATORY
UNIVERSITY OF CALIFORNIA
BERKELEY, CALIFORNIA 94720